REPRESENTATION BALANCING WITH DECOMPOSED PATTERNS FOR TREATMENT EFFECT ESTIMATION

Anonymous authors
Paper under double-blind review

ABSTRACT

Estimating treatment effects from observational data is subject to a problem of covariate shift caused by selection bias. Recent studies have attempted to mitigate this problem by group distance minimization, that is, balancing the distribution of representations between the treated and controlled groups. The rationale behind this is that learning balanced representations while preserving the predictive power of factual outcomes is expected to generalize to counterfactual inference. Inspired by this, we propose a new approach to better capture the patterns that contribute to representation balancing and outcome prediction. Specifically, we derive a theoretical bound that naturally ties the notion of propensity confusion to representation balancing, and further transform the balancing Patterns into Decompositions of Individual propensity confusion and Group distance minimization (PDIG). Moreover, we propose to decompose proxy features into Patterns of Pre-balancing and Balancing Representations (PPBR), as it is insufficient if only balanced representations are considered in outcome prediction. Extensive experiments on simulation and benchmark data confirm not only PDIG leads to mutual reinforcement between individual propensity confusion and group distance minimization, but also PPBR brings improvement to outcome prediction, especially to counterfactual inference. We believe these findings are heuristics for further investigation of what affects the generalizability of representation balancing models in counterfactual estimation.

1 INTRODUCTION

In the context of the ubiquity of personalized decision-making, causal inference has sparked a surge of research exploring causal machine learning in many disciplines, including economics and statistics (Wager & Athey, 2018; Athey & Wager, 2019; Farrell, 2015; Chernozhukov et al., 2018; Huang et al., 2021), healthcare (Qian et al., 2021; Bica et al., 2021a;b), and commercial applications (Guo et al., 2020b;c; Chu et al., 2021). The main problem of causal inference is the *treatment effect estimation*, which is tied to a fundamental hypothetical question: What would be the outcome if one received an alternative treatment? Answering this question requires the knowledge of *counterfactual outcomes*, but they can only be inferred from observational data, not directly obtained.

Selection bias presents a major challenge for estimating counterfactual outcomes (Guo et al., 2020a; Zhang et al., 2020; Yao et al., 2021). This problem is caused by the non-random treatment assignment, that is, treatment (e.g., vaccination) is usually determined by covariates (e.g., age) that also affect the outcome (e.g., infection rate) (Huang et al., 2022b). The probability of a person receiving treatment is well known as the *propensity score*, and the difference between each person's propensity score can inherently lead to a covariate shift problem, i.e., the distribution of covariates in the treated units is substantially different from that in the controlled ones. The covariate shift issue makes it more difficult to infer counterfactual outcomes from observational data (Yao et al., 2018; Hassanpour & Greiner, 2019a).

Recently, a line of representation balancing works has sought to alleviate the covariate shift problem by balancing the distribution between the treated group and the controlled group in the representation space (Shalit et al., 2017; Johansson et al., 2022). As a matter of fact, what exactly determines the generalizability of a model in terms of counterfactual estimation is still inexplicit, but the rational insight behind these works is that the counterfactual estimation should rest on the accuracy of

factual estimation while enforcing minimization of distributional discrepancy measured by the Integral Probability Metric (IPM) between the treated and controlled units. In previous representation balancing works, Wasserstein distance (Cuturi & Doucet, 2014) is the most widely-adopted metric for group distance minimization (Shalit et al., 2017; Huang et al., 2022a; Zhou et al., 2022). In contrast, $\mathcal{H}$-divergence has still received little attention in causal representation learning though it is a typical distance metric in other representation learning fields (Ben-David et al., 2006; 2010). One of our goals is to show that $\mathcal{H}$-divergence can be naturally associated with the concept of *propensity confusion*, highlighting the role of propensity scores in interpretable representation balancing.

Simultaneously, eliminating the covariate shift does not necessarily guarantee a better estimate of treatment effect. Previous representation balancing approaches encourage their models to predict outcomes by the balanced representations, but such a technique has been shown to inadvertently weaken the predictive power of the outcome function if representations are improperly balanced (Zhang et al., 2020; Assaad et al., 2021; Huang et al., 2022a). Therefore, another goal of this paper is to explore a framework that preserves the predictive power of outcome modeling by capturing both pre-balancing and balancing patterns.

To address the aforementioned issues and gain more insights into causal representation balancing, we propose a decomposition network architecture called DIGNet. The **contributions** are threefold: (1) We interpret representation balancing as a concept of propensity confusion and derive corresponding theoretical results based on $\mathcal{H}$-divergence to ensure its rationality; (2) DIGNet transforms the balancing Patterns into Decompositions of Individual propensity confusion and Group distance minimization (*PDIG*) to capture patterns beneficial to representation balancing, and we empirically find that the PDIG structure enables individual propensity confusion and group distance minimization to reinforce each other; (3) DIGNet decomposes representative features into Patterns of Pre-balancing and Balancing Representations (*PPBR*) to preserve patterns contributing to outcome modeling, and we experimentally confirm that the PPBR approach brings improvement to outcome prediction, especially to counterfactual inference.

1.1 Related Work

The presence of a covariate shift problem stimulates the line of representation balancing works (Johansson et al., 2016; Shalit et al., 2017; Johansson et al., 2022). These works aim to balance the distributions of representations between treated and controlled groups and simultaneously try to maintain representations predictive of factual outcomes. This idea is closely connected with domain adaptation. In particular, the individual treatment effect (ITE) error bound based on Wasserstein distance is similar to the generalization bound in Ben-David et al. (2010); Long et al. (2014); Shen et al. (2018). In addition to Wasserstein distance-based model, this paper derives a new ITE error bound based on $\mathcal{H}$-divergence (Ben-David et al., 2006; 2010; Ganin et al., 2016).

Another recent line of work investigates efficient neural network structures for treatment effect estimation. Kuang et al. (2017); Hassanpour & Greiner (2019b) extract the original covariates into treatment-specific factors, outcome-specific factors, and confounding factors; X-learner (Künzel et al., 2019) and R-learner (Nie & Wager, 2021) are developed beyond the classic S-learner and T-learner; Curth & van der Schaar (2021) leverage structures for end-to-end learners to counteract the inductive bias towards treatment effect estimation, as motivated by Makar et al. (2020).

The proposed DIGNet model is built on the PDIG structure and the PPBR approach. The PDIG structure is motivated by multi-task learning, where we design a framework incorporating two specific balancing patterns that share the same pre-balancing patterns. The PPBR approach is inspired by Zhang et al. (2020); Assaad et al. (2021); Huang et al. (2022a), where the authors argue that improperly balanced representations can be detrimental predictors for outcome modeling, since such representations can lose the original information that contributes to outcome prediction. Other representation learning methods relevant to treatment effect estimation include Louizos et al. (2017); Yao et al. (2018); Yoon et al. (2018); Shi et al. (2019); Du et al. (2021).

2 Preliminaries

Notations. Suppose there are the N i.i.d. random variable samples $\mathcal{D} = \{(\mathbf{X}_i, T_i, Y_i)\}_{i=1}^N$ with observed realizations $\{(\mathbf{x}_i, t_i, y_i)\}_{i=1}^N$, where there are N_1 treated units and N_0 controlled units. For

each unit i, $\mathbf{X}_i \in \mathcal{X} \subset \mathbb{R}^d$ denotes d-dimensional covariates and $T_i \in \{0,1\}$ denotes the binary treatment, with $e(\mathbf{x}_i) := p(T_i = 1 \mid \mathbf{X}_i = \mathbf{x}_i)$ defined as the propensity score (Rosenbaum & Rubin, 1983). Potential outcome framework (Rubin, 2005) defines the potential outcomes $Y^1, Y^0 \in \mathcal{Y} \subset \mathbb{R}$ for treatment $T = 1$ and $T = 0$, respectively. We let the observed outcome (factual outcome) be $Y = T \cdot Y^1 + (1-T) \cdot Y^0$. For $t \in \{0,1\}$, let $\tau^t(\mathbf{x}) := \mathbb{E}\left[Y^t \mid \mathbf{X} = \mathbf{x}\right]$ be a function of Y^t w.r.t. $\mathbf{X}$, then our goal is to estimate the individual treatment effect (ITE) $\tau(\mathbf{x}) := \mathbb{E}\left[Y^1 - Y^0 \mid \mathbf{X} = \mathbf{x}\right] = \tau^1(\mathbf{x}) - \tau^0(\mathbf{x})$, and the average treatment effect (ATE) $\tau_{ATE} := \mathbb{E}\left[Y^1 - Y^0\right] = \int_{\mathcal{X}} \tau(\mathbf{x}) p(\mathbf{x}) d\mathbf{x}$.

2.1 Problem setup

In causal representation balancing works, we denote representation space by $\mathcal{R} \subset \mathbb{R}^d$, and $\Phi : \mathcal{X} \to \mathcal{R}$ is assumed to be a twice-differentiable, one-to-one and invertible function with its inverse $\Psi : \mathcal{R} \to \mathcal{X}$ such that $\Psi(\Phi(\mathbf{x})) = \mathbf{x}$. The densities of the treated and controlled covariates are denoted by $p_{\mathbf{x}}^{T=1} = p^{T=1}(\mathbf{x}) := p(\mathbf{x} \mid T = 1)$ and $p_{\mathbf{x}}^{T=0} = p^{T=0}(\mathbf{x}) := p(\mathbf{x} \mid T = 0)$, respectively. Correspondingly, the densities of the treated and controlled covariates in the representation space are denoted by $p_{\Phi}^{T=1} = p_{\Phi}^{T=1}(\mathbf{r}) := p_{\Phi}(\mathbf{r} \mid T = 1)$ and $p_{\Phi}^{T=0} = p_{\Phi}^{T=0}(\mathbf{r}) := p_{\Phi}(\mathbf{r} \mid T = 0)$, respectively.

Our study is based on the potential outcome framework (Rubin, 2005). Assumption 1 states standard and necessary assumptions to ensure treatment effects are identifiable. Before proceeding with theoretical analysis, we also present the necessary terms and definitions in Definition 1.

Assumption 1 (Consistency, Overlap, and Unconfoundedness) *Consistency: If the treatment is t, then the observed outcome equals Y^t. Overlap: The propensity score is bounded away from 0 to 1: $0 < e(\mathbf{x}) < 1$. Unconfoundedness: $Y^t \perp\!\!\!\perp T \mid \mathbf{X}$, $\forall t \in \{0,1\}$.*

Definition 1 *Let $h : \mathcal{R} \times \{0,1\} \to \mathcal{Y}$ be an hypothesis defined over the representation space $\mathcal{R}$ such that $h(\Phi(\mathbf{x}), t)$ estimates y^t, and $L : \mathcal{Y} \times \mathcal{Y} \to \mathbb{R}_+$ be a loss function (e.g., $L(y, y') = (y - y')^2$). If we define the expected loss for $(\mathbf{x}, t)$ as $\ell_{h,\Phi}(\mathbf{x}, t) = \int_{\mathcal{Y}} L(y^t, h(\Phi(\mathbf{x}), t)) p(y^t|\mathbf{x}) dy^t$, we then have factual and counterfactual losses, as well as them on the treated and controlled:*

$$\epsilon_F(h, \Phi) = \int_{\mathcal{X} \times \{0,1\}} \ell_{h,\Phi}(\mathbf{x}, t) p(\mathbf{x}, t) d\mathbf{x} dt, \quad \epsilon_{CF}(h, \Phi) = \int_{\mathcal{X} \times \{0,1\}} \ell_{h,\Phi}(\mathbf{x}, t) p(\mathbf{x}, 1-t) d\mathbf{x} dt,$$

$$\epsilon_F^{T=1}(h, \Phi) = \int_{\mathcal{X}} \ell_{h,\Phi}(\mathbf{x}, 1) p^{T=1}(\mathbf{x}) d\mathbf{x}, \qquad \epsilon_F^{T=0}(h, \Phi) = \int_{\mathcal{X}} \ell_{h,\Phi}(\mathbf{x}, 0) p^{T=0}(\mathbf{x}) d\mathbf{x},$$

$$\epsilon_{CF}^{T=1}(h, \Phi) = \int_{\mathcal{X}} \ell_{h,\Phi}(\mathbf{x}, 1) p^{T=0}(\mathbf{x}) d\mathbf{x}, \qquad \epsilon_{CF}^{T=0}(h, \Phi) = \int_{\mathcal{X}} \ell_{h,\Phi}(\mathbf{x}, 0) p^{T=1}(\mathbf{x}) d\mathbf{x}.$$

If we let $f(\mathbf{x}, t)$ be $h(\Phi(\mathbf{x}), t)$, where $f : \mathcal{X} \times \{0,1\} \to \mathcal{Y}$ is a prediction function for outcome, then the estimated ITE over f is defined as $\hat{\tau}_f(\mathbf{x}) := f(\mathbf{x}, 1) - f(\mathbf{x}, 0)$. Finally, a better treatment effect estimation can be reformulated as a smaller error in Precision in the expected Estimation of Heterogeneous Effect (PEHE):

$$\epsilon_{PEHE}(f) = \int_{\mathcal{X}} L(\hat{\tau}_f(\mathbf{x}) - \tau(\mathbf{x})) p(\mathbf{x}) d\mathbf{x}. \tag{1}$$

Here, $\epsilon_{PEHE}(f)$ can also be denoted by $\epsilon_{PEHE}(h, \Phi)$ if we let $f(\mathbf{x}, t)$ be $h(\Phi(\mathbf{x}), t)$.

3 Theoretical Results

In this section, we first prove ϵ_{PEHE} is bounded by ϵ_F and ϵ_{CF} in Lemma 1. Next, we revisit the upper bound (Theorem 1) concerning the group distance minimization guided method in Section 3.1. Section 3.2 further discusses the theoretical results of the proposed individual propensity confusion guided method in Theorem 2. Proofs and additional theoretical results are deferred to Appendix.

Lemma 1 *Let functions h and Φ be as defined in Definition 1, and L be the squared loss function. Recall that $\tau^t(\mathbf{x}) = \mathbb{E}\left[Y^t \mid \mathbf{X} = \mathbf{x}\right]$. Defining $\sigma_y^2 = \min\{\sigma_{y^t}^2(p(\mathbf{x}, t)), \sigma_{y^t}^2(p(\mathbf{x}, 1-t))\}$ $\forall t \in \{0,1\}$, where $\sigma_{y^t}^2(p(\mathbf{x}, t)) = \int_{\mathcal{X} \times \{0,1\} \times \mathcal{Y}} (y^t - \tau^t(\mathbf{x}))^2 p(y^t|\mathbf{x}) p(\mathbf{x}, t) dy^t d\mathbf{x} dt$, we have*

$$\epsilon_{PEHE}(h, \Phi) \leq 2(\epsilon_{CF}(h, \Phi) + \epsilon_F(h, \Phi) - 2\sigma_y^2).$$

Note that similar results will hold as long as L takes forms that satisfy the triangle inequality, but is not limited to the squared loss. For instance, we give the result for absolute loss in Lemma 6 in Appendix. This extends the result shown in Shalit et al. (2017) that L only takes the squared loss.

3.1 GNET: GROUP DISTANCE MINIMIZATION GUIDED REPRESENTATION BALANCING

Previous group distance minimization guided approaches seek representation balancing by minimizing the distance measured by the Integral Probability Metric (IPM) defined in Definition 2.

Definition 2 *Let $\mathcal{G}$ be a function family consisting of functions $g : \mathcal{S} \to \mathbb{R}$. For a pair of distributions p_1, p_2 over $\mathcal{S}$, the Integral Probability Metric is defined as*

$$IPM_{\mathcal{G}}(p_1, p_2) := sup_{g \in \mathcal{G}} \left| \int_{\mathcal{S}} g(s)(p_1(s) - p_2(s))ds \right|.$$

If $\mathcal{G}$ is the family of 1-Lipschitz functions, we can obtain the so-called 1-Wasserstein distance, denoted by $Wass(p_1, p_2)$ (Sriperumbudur et al., 2012). Next, we give the bounds for counterfactual error ϵ_{CF} and ITE error ϵ_{PEHE} using Wasserstein distance in Theorem 1.

Theorem 1 *Let h, Φ, Ψ, $p_\Phi^{T=1}$, and $p_\Phi^{T=0}$ be as defined before. Let L be the squared loss, $u := Pr(T = 1)$, and $\mathcal{G}$ be the family of 1-Lipschitz functions. Assuming that there exists a constant $B_\Phi \geq 0$ such that $g_{\Phi,h}(\mathbf{r}, t) := \frac{1}{B_\Phi} \cdot \ell_{h,\Phi}(\Psi(\mathbf{r}), t) \in \mathcal{G}$ for fixed $t \in \{0, 1\}$, we then have*

$$\epsilon_{CF}(h, \Phi) \leq (1 - u) \cdot \epsilon_F^{T=1}(h, \Phi) + u \cdot \epsilon_F^{T=0}(h, \Phi) + B_\Phi \cdot Wass(p_\Phi^{T=1}, p_\Phi^{T=0}), \tag{2}$$

$$\epsilon_{PEHE}(h, \Phi) \leq 2(\epsilon_F^{T=1}(h, \Phi) + \epsilon_F^{T=0}(h, \Phi) + B_\Phi \cdot Wass(p_\Phi^{T=1}, p_\Phi^{T=0}) - 2\sigma_y^2). \tag{3}$$

Theorem 1 will be identical to Shalit et al. (2017) if L is the squared loss. Note, however, that similar results for Theorem 1 still hold as long as L takes forms that satisfy the triangle inequality. For instance, we give the result for absolute loss in Theorem 3 in Appendix. We refer to the model as **GNet** (aka CFR-Wass in Shalit et al. (2017)) since it is based on group distance minimization.

3.2 INET: INDIVIDUAL PROPENSITY CONFUSION GUIDED REPRESENTATION BALANCING

The propensity score is recognized central to treatment effect estimation because it characterizes the probability that one receives treatment (Rosenbaum & Rubin, 1983). Therefore, in addition to group distance minimization, the propensity score can be naturally used to identify if representations are adequately balanced, since representation balancing can be intuitively interpreted as propensity confusion, that is, when it is hard to distinguish whether each unit in the representation space is treated or controlled, the representations are thought adequately balanced. In section 4.1, we will demonstrate how minimizing $\mathcal{H}$-divergence (Definition 3) is empirically related to propensity confusion. Below, we first derive an ITE bound in Theorem 2 based on $\mathcal{H}$-divergence.

Definition 3 *Given a pair of distributions p_1, p_2 over $\mathcal{S}$, and a hypothesis binary function class $\mathcal{H}$, the $\mathcal{H}$-divergence between p_1 and p_2 is defined as*

$$d_{\mathcal{H}}(p_1, p_2) := 2sup_{\eta \in \mathcal{H}} \left| Pr_{p_1}[\eta(s) = 1] - Pr_{p_2}[\eta(s) = 1] \right|. \tag{4}$$

Theorem 2 *Let h, Φ, Ψ, $p_\Phi^{T=1}$, and $p_\Phi^{T=0}$ be as defined before. Let L be the squared loss, $u := Pr(T = 1)$, and $\mathcal{H}$ be the family of binary functions. Assuming that there exists a constant $K \geq 0$ such that $\int_{\mathcal{Y}} L(y, y')dy \leq K \ \forall y' \in \mathcal{Y}$, we then have*

$$\epsilon_{CF}(h, \Phi) \leq (1 - u) \cdot \epsilon_F^{T=1}(h, \Phi) + u \cdot \epsilon_F^{T=0}(h, \Phi) + \frac{K}{2} d_{\mathcal{H}}(p_\Phi^{T=1}, p_\Phi^{T=0}), \tag{5}$$

$$\epsilon_{PEHE}(h, \Phi) \leq \epsilon_F^{T=1}(h, \Phi) + \epsilon_F^{T=0}(h, \Phi) + \frac{K}{2} d_{\mathcal{H}}(p_\Phi^{T=1}, p_\Phi^{T=0}) - 2\sigma_y^2. \tag{6}$$

We can apply similar arguments in proving Theorem 2 to obtain the corresponding upper bounds as long as L takes forms that satisfy the triangle inequality. For instance, the result for absolute loss and the proof of Theorem 2 are given in Theorem 4 in Appendix. We refer to the model as **INet** since it is based on individual propensity confusion.

4 METHOD

In this section, we will demonstrate how Theorem 2 is associated with propensity confusion, and further suggest a decomposition network DIGNet based on GNet and INet. Section 4.1 presents the objectives of standard representation balancing models, GNet and INet. Section 4.2 introduces PDIG and PPBR components for the representation balancing with decomposed patterns scheme, and gives the final objective of the proposed model DIGNet.

4.1 REPRESENTATION BALANCING WITHOUT DECOMPOSED PATTERNS

In representation balancing models, given the input data tuples $(\mathbf{x}, \mathbf{t}, \mathbf{y}) = \{(\mathbf{x}_i, t_i, y_i)\}_{i=1}^N$, the original covariates $\mathbf{x}$ are extracted by some representation function $\Phi(\cdot)$, and representations $\Phi(\mathbf{x})$ are then fed into the outcome functions $h^1(\cdot) := h(\cdot, 1)$ and $h^0(\cdot) := h(\cdot, 0)$ that estimate the potential outcome y^1 and y^0, respectively. Finally, the factual outcome can be predicted by $h^t(\cdot) = th^1(\cdot) + (1-t)h^0(\cdot)$, and the corresponding outcome loss is

$$\mathcal{L}_y(\mathbf{x}, \mathbf{t}, \mathbf{y}; \Phi, h^t) = \frac{1}{N} \sum_{i=1}^{N} L(h^t(\Phi(\mathbf{x}_i)), y_i). \tag{7}$$

If a model does not have decomposition modes like GNet and INet, both outcome prediction and representation balancing will rely on the extracted features $\Phi(\mathbf{x})$. Below we will introduce the objectives of GNet and INet.

Objective of GNet. GNet learns the balancing patterns over Φ by minimizing the group distance loss $\mathcal{L}_G(\mathbf{x}, \mathbf{t}; \Phi) = Wass\left(\{\Phi(\mathbf{x}_i)\}_{i:t_i=0}, \{\Phi(\mathbf{x}_i)\}_{i:t_i=1}\right)$. If the original covariates $\mathbf{x}$ are extracted by the feature extractor $\Phi_E(\cdot)$, then the final objective of GNet is

$$\min_{\Phi_E, h^t} \quad \mathcal{L}_y(\mathbf{x}, \mathbf{t}, \mathbf{y}; \Phi_E, h^t) + \alpha_1 \mathcal{L}_G(\mathbf{x}, \mathbf{t}; \Phi_E). \tag{8}$$

For the convenience of the reader, we illustrate the structure of GNet in Figure 1(a).

Objective of INet. Next, we detail how Theorem 2 is related to propensity confusion and give the objective of INet. Let $\mathbb{I}(a)$ be an indicator function that gives 1 if a is true, and $\mathcal{H}$ be the family of binary functions as defined in Theorem 2. The representation balancing seeks to ahieve a smaller empirical $\mathcal{H}$-divergence $\hat{d}_{\mathcal{H}}(p_\Phi^{T=1}, p_\Phi^{T=0})$ such that

$$\hat{d}_{\mathcal{H}}(p_\Phi^{T=1}, p_\Phi^{T=0}) = 2\left(1 - \min_{\eta \in \mathcal{H}} \left[\frac{1}{N_0} \sum_{i:t_i=0}^{N_0} \mathbb{I}[\eta(\Phi(\mathbf{x}_i)) = 0] + \frac{1}{N_1} \sum_{i:t_i=1}^{N_1} \mathbb{I}[\eta(\Phi(\mathbf{x}_i)) = 1]\right]\right). \tag{9}$$

The "min" part in equation 9 indicates that the optimal classifier $\eta^* \in \mathcal{H}$ minimizes the classification error between the estimated treatment $\eta^*(\Phi(\mathbf{x}_i))$ and the observed treatment t_i, i.e., discriminating whether $\Phi(\mathbf{x}_i)$ is controlled ($T = 0$) or treated ($T = 1$). As a result, $\hat{d}_{\mathcal{H}}(p_\Phi^{T=1}, p_\Phi^{T=0})$ will be large if η^* can easily distinguish whether $\Phi(\mathbf{x}_i)$ is treated or controlled, i.e., the optimal classification error is small. In contrast, $\hat{d}_{\mathcal{H}}(p_\Phi^{T=1}, p_\Phi^{T=0})$ will be small if it is hard for η^* to determine whether $\Phi(\mathbf{x}_i)$ is treated or controlled, i.e., the optimal classification error is large. Therefore, the prerequisite of a small $\mathcal{H}$-divergence is to find a map Φ such that any classifier $\eta \in \mathcal{H}$ will get confused about the probability of $\Phi(\mathbf{x}_i)$ being treated or controlled. To achieve this goal, we first define a discriminator $\pi(\mathbf{r}) : \mathcal{R} \to [0, 1]$ that estimates the propensity score of $\mathbf{r}$. The classification error for the ith individual can be empirically approximated by the cross-entropy loss between $\pi(\Phi(\mathbf{x}_i))$ and t_i:

$$\mathcal{L}_t(t_i, \pi(\Phi(\mathbf{x}_i))) = -\left[t_i \log \pi(\Phi(\mathbf{x}_i)) + (1 - t_i) \log(1 - \pi(\Phi(\mathbf{x}_i)))\right]. \tag{10}$$

To minimize the classification error in equation 9, we aim to find an optimal discriminator π^* such that π^* maximizes the probability that treatment is correctly classified of the total population:

$$\max_{\pi \in \mathcal{H}} \mathcal{L}_I(\mathbf{x}, \mathbf{t}; \Phi, \pi) = \max_{\pi \in \mathcal{H}} \left[-\frac{1}{N_0} \sum_{i:t_i=0}^{N_0} \mathcal{L}_t(t_i, \pi(\Phi(\mathbf{x}_i))) - \frac{1}{N_1} \sum_{i:t_i=1}^{N_1} \mathcal{L}_t(t_i, \pi(\Phi(\mathbf{x}_i)))\right]. \tag{11}$$

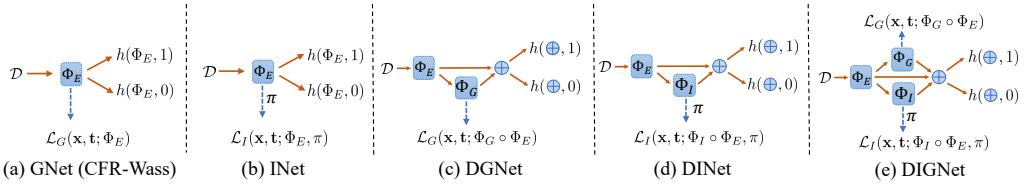

(a) GNet (CFR-Wass) (b) INet (c) DGNet (d) DINet (e) DIGNet

Figure 1: Illustrations of the network architecture of the five models studied in Section 5.

Given the feature extractor $\Phi_E(\cdot)$, the objective of INet can be formulated as a min-max game:

$$\min_{\Phi_E, h^t} \max_{\pi} \quad \mathcal{L}_y(\mathbf{x}, \mathbf{t}, \mathbf{y}; \Phi_E, h^t) + \alpha_2 \mathcal{L}_I(\mathbf{x}, \mathbf{t}; \Phi_E, \pi). \tag{12}$$

As stated in equation 12, INet achieves the representation balancing through a min-max formulation. In the maximization, the discriminator π is trained to maximize the probability that treatment is correctly classified. This forces $\pi(\Phi_E(\mathbf{x}_i))$ closer to the true propensity score $e(\mathbf{x}_i)$. In the minimization, the feature extractor Φ_E is trained to fool the discriminator π. This confuses π such that $\pi(\Phi_E(\mathbf{x}_i))$ cannot correctly specify the true propensity score $e(\mathbf{x}_i)$. Eventually, the representations are balanced as it is difficult for π to determine the propensity of $\Phi(\mathbf{x}_i)$ being treated or controlled. For the convenience of the reader, we illustrate the structure of INet in Figure 1(b).

4.2 Representation Balancing with Decomposed Patterns

PDIG. Previous demonstrations have shown that GNet is thriving and widely adopted, while INet is meaningful and interpretable. Nevertheless, there is no consensus on the absolute best approach, as each method has its strengths and weaknesses. To this end, we expect to capture more effective balancing patterns by turning the balancing Patterns into Decompositions of Individual propensity confusion and Group distance minimization (PDIG). More specifically, the covariates $\mathbf{x}$ are extracted by the feature extractor $\Phi_E(\cdot)$, and then $\Phi_E(\mathbf{x})$ are fed into the balancing networks $\Phi_G(\cdot)$ and $\Phi_I(\cdot)$ for group distance minimization and individual propensity confusion, respectively. Finally, the losses for the two separate balancing patterns are

$$\min_{\Phi_G} \quad \mathcal{L}_G(\mathbf{x}, \mathbf{t}; \Phi_G \circ \Phi_E), \qquad \min_{\Phi_I} \max_{\pi} \quad \mathcal{L}_I(\mathbf{x}, \mathbf{t}; \Phi_I \circ \Phi_E, \pi). \tag{13}$$

Here, $\circ$ denotes the composition of two functions, indicating that $\Phi(\cdot)$ in $\mathcal{L}_G(\mathbf{x}, \mathbf{t}; \Phi)$ and $\mathcal{L}_I(\mathbf{x}, \mathbf{t}; \Phi, \pi)$ are replaced by $\Phi_G(\Phi_E(\cdot))$ and $\Phi_I(\Phi_E(\cdot))$, respectively.

PPBR. Motivated by the discussion in Section 1, we aim to design a framework that is capable of capturing Patterns of Pre-balancing and Balancing Representations (PPBR). First, the representation balancing patterns $\Phi_G(\Phi_E(\mathbf{x}))$ and $\Phi_I(\Phi_E(\mathbf{x}))$ are learned over Φ_G and Φ_I, while Φ_E is remained fixed as pre-balancing patterns. Furthermore, we concatenate the balancing representations $\Phi_G(\Phi_E(\mathbf{x}))$ and $\Phi_I(\Phi_E(\mathbf{x}))$ with the pre-balancing representations $\Phi_E(\mathbf{x})$ as attributes for outcome prediction. As a result, the proxy features used for outcome predictions are $\Phi_E(\mathbf{x}) \oplus \Phi_G(\Phi_E(\mathbf{x})) \oplus \Phi_I(\Phi_E(\mathbf{x}))$, where $\oplus$ indicates the concatenation by column. For example, if $\mathbf{a} = [1, 2]$ and $\mathbf{b} = [3, 4]$, then $\mathbf{a} \oplus \mathbf{b} = [1, 2, 3, 4]$.

Objective of DIGNet. Combining with PDIG and PPBR, we develop a new model architecture, DIGNet, as illustrated in Figure 1(e). The objective of DIGNet is separated into four stages:

$$\min_{\Phi_G} \quad \alpha_1 \mathcal{L}_G(\mathbf{x}, \mathbf{t}; \Phi_G \circ \Phi_E), \tag{14}$$

$$\max_{\pi} \quad \alpha_2 \mathcal{L}_I(\mathbf{x}, \mathbf{t}; \Phi_I \circ \Phi_E, \pi), \tag{15}$$

$$\min_{\Phi_I} \quad \alpha_2 \mathcal{L}_I(\mathbf{x}, \mathbf{t}; \Phi_I \circ \Phi_E, \pi), \tag{16}$$

$$\min_{\Phi_E, \Phi_I, \Phi_G, h^t} \quad \mathcal{L}_y(\mathbf{x}, \mathbf{t}, \mathbf{y}; \Phi_E \oplus (\Phi_I \circ \Phi_E) \oplus (\Phi_G \circ \Phi_E), h^t). \tag{17}$$

Within each iteration, DIGNet manages to minimize the group distance via equation 14, and plays an adversarial game to achieve propensity confusion through equation 15 and equation 16. In equation 17, DIGNet updates both the pre-balancing and balancing patterns Φ_E, Φ_I, Φ_G along with the outcome function f^t to minimize the outcome prediction loss.

DGNet and DINet. For further ablation studies, we also propose two models, DGNet and DINet. The two models can be considered as either DIGNet without PDIG, or GNet and INet with PPBR. The structures of DGNet and DINet are shown in Figure 1(c) and Figure 1(d), and the objectives of DGNet and DINet are deferred to Section A.5 in Appendix.

5 EXPERIMENTS

In non-randomized observational data, the ground truth of treatment effects is inaccessible due to the lack of counterfactuals. Therefore, we use simulated data and semi-synthetic benchmark data to test the performance of our methods and other baseline models. In this section, we mainly investigate two questions: **Q1.** Compared to DGNet and DINet without the PDIG structure, can DIGNet with the PDIG structure achieve a better representation balancing task? **Q2.** Are DGNet and DINet that involve PPBR capable of improving the performance on outcome prediction compared with standard representation balancing models such as GNet and INet?

5.1 EXPERIMENTAL SETTINGS

Simulation data. Previous causal inference works assess the model effectiveness by varying the distribution imbalance of covariates in treated and controlled groups at different levels (Yao et al., 2018; Yoon et al., 2018; Du et al., 2021). As suggested in Assaad et al. (2021), we draw 1000 observational data points from the following data generating strategy:

$$\mathbf{X}_i \sim \mathcal{N}(\mathbf{0}, \sigma^2 \cdot [\rho \mathbf{1}_p \mathbf{1}_p^{'} (1-\rho)\mathbf{I}_p]), \quad T_i \mid \mathbf{X}_i \sim \text{Bernoulli}(1+\exp(-\gamma \mathbf{X}_i)),$$
$$Y_i^0 = \boldsymbol{\beta}_{\mathbf{0}}' \mathbf{X}_i + \xi_i, \qquad Y_i^1 = \boldsymbol{\beta}_{\mathbf{1}}' \mathbf{X}_i + \xi_i, \qquad \xi_i \sim \mathcal{N}(0,1).$$

Here, $\mathbf{1}_p$ denotes the p-dimensional all-ones vector and $\mathbf{I}_p$ denotes the identity matrix of size p. We fix $p = 10, \rho = 0.3, \sigma^2 = 2, \boldsymbol{\beta}_{\mathbf{0}}' = [0.3, ..., 0.3], \boldsymbol{\beta}_{\mathbf{1}}' = [1.3, ..., 1.3]$ and vary $\gamma \in \{0.25, 0.5, 0.75, 1, 1.5, 2, 3\}$ to yield different level of selection bias. As seen in Figure 5 in Appendix, selection bias becomes more severe with γ increasing. For each γ, we repeat the above data generating process to generate 30 different datasets, with each dataset split by the ratio of $56\%/24\%/20\%$ as training/validation/test sets.

Semi-synthetic data The IHDP dataset is introduced by Hill (2011). This dataset consists of 747 samples with 25-dimensional covariates collected from real-world randomized experiments. Selection bias is created by removing some of treated samples. The goal is to estimate the effect of special visits (treatment) on cognitive scores (outcome). The potential outcomes are generated using the NPCI package Dorie (2021). We use the same 1000 datasets as used in Shalit et al. (2017), with each dataset split by the ratio of $63\%/27\%/10\%$ as training/validation/test sets.

Models and metrics. In simulation experiments, we perform comprehensive comparisons between INet, GNet, DINet, DGNet, and DIGNet in terms of the mean and standard error for the following metrics: ϵ_{PEHE}, ϵ_{CF}, and ϵ_F with L defined in Definition 1 being the squared loss, as well as the empirical approximations of $Wass(p_\Phi^{T=1}, p_\Phi^{T=0})$ and $d_{\mathcal{H}}(p_\Phi^{T=1}, p_\Phi^{T=0})$ (denoted by $Wass$ and $\hat{d}_{\mathcal{H}}$, respectively). Note that as shown in Figure 1, $Wass$ is over Φ_E for GNet while over Φ_G for DGNet and DIGNet; $\hat{d}_{\mathcal{H}}$ is over Φ_E for INet while over Φ_I for DINet and DIGNet. To analyze the source of gain, we fairly compare models by ensuring that each model shares the same hyperparameters, e.g., learning rate, the number of layers and units for $(\Phi_E, \Phi_G, \Phi_I, f^t)$, and (α_1, α_2). Note that we apply an early stopping rule to all models as Shalit et al. (2017) do. In IHDP experiment, we use ϵ_{PEHE}, as well as an additional metric $\epsilon_{ATE} = |\hat{\tau}_{ATE} - \tau_{ATE}|$ to evaluate performances of various causal models (see them in Table 3). More descriptions of the implementation are detailed in Section A.4 of Appendix.

5.2 RESULTS AND ANALYSIS

Varying selection bias. We first make a general comparison between the models on datasets when the degree of covariate imbalance increases, and the relevant results are shown in Figure 2. There are three main observations: (1) DIGNet attains the lowest ϵ_{PEHE} across all datasets, while GNet

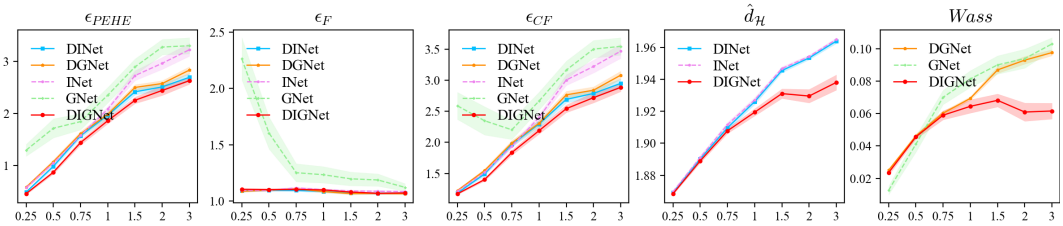

Figure 2: Plots of model performances on test set for different metrics as γ varies in $\{0.25, 0.5, 0.75, 1, 1.5, 2, 3\}$. Each graph shows the average of 30 runs with standard errors shaded.

performs worse than other models; (2) DINet and DGNet outperform INet and GNet regarding ϵ_{CF} and ϵ_{PEHE}; (3) INet, DINet, and DGNet perform similarly to DIGNet on factual outcome estimations (ϵ_F), but cannot compete with DIGNet in terms of counterfactual estimations (ϵ_{CF}); (4) DIGNet achieves smaller $\hat{d}_{\mathcal{H}}$ (or $Wass$) than DINet and INet (or DGNet and GNet), especially when the covariate shift problem is severe (e.g., when $\gamma > 1$).

In conclusion, the finding (2) reveals that *(i) the PPBR approach improves the predictive power of outcomes, especially for counterfactual outcomes*; and the findings (3) and (4) reveal that *(ii) the PDIG structure conduces to making group distance minimization and individual propensity confusion complementary and mutually reinforcing.*

Source of gain. To further investigate the above findings, we choose the case with high selection bias ($\gamma = 3$) to explore the source of gain for PDIG and PPBR. We report model performances (mean $\pm$ std) averaged over 30 training and test sets in Table 1 and plot specific metrics of 30 runs on test set in Figure 3 and Figure 4. Below we discuss the source of gain in detail.

(1) Ablation study for PDIG: The PDIG structure is manifest to be effective in capturing balancing patterns. According to Figure 2, although DIGNet, DINet, and DGNet have comparable estimates of factual outcomes (ϵ_F), DIGNet can achieve more balanced representations regardless of the discrepancy is measured by $\hat{d}_{\mathcal{H}}$ or $Wass$. In particular, by comparing DIGNet with DGNet and DINet in Figure 3, we find that the PDIG structure does not affect the factual outcome estimation (ϵ_F). Nevertheless, DIGNet achieves smaller $\hat{d}_{\mathcal{H}}$ with a $|1.94/1.96 - 1| = 1.0\%$ reduction (or $Wass$ with a $|0.06/0.10 - 1| = 40\%$ reduction) compared with DINet (or DGNet). This indicates that PDIG enables group distance minimization and individual propensity confusion to complement and reinforce each other, thereby learning better balancing patterns. This bring benefits with regard to counterfactual estimation. In particular, DIGNet reduces ϵ_{CF} by $|2.89/2.95 - 1| = 2.0\%$ and $|2.89/3.08 - 1| = 6.2\%$ for DINet and DGNet, respectively. Thanks to the efficacy of PDIG in capturing balancing patterns, DIGNet shows superiority in treatment effect estimation (ϵ_{PEHE} and ϵ_{ATE}) compared to DGNet and DINet, as seen in Table 1.

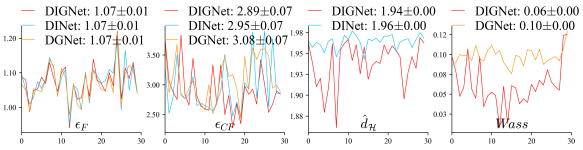

Figure 3: Plots of model performances on test set for ϵ_F, ϵ_{CF}, $\hat{d}_{\mathcal{H}}$, and $Wass$ when $\gamma = 3$. Each graph plots the metric for 30 runs. Mean $\pm$ std of each metric averaged across 30 runs are reported on the top.

(2) Ablation study for PPBR: The PPBR approach plays an essential role in outcome prediction, especially counterfactual inference. From Figure 4, we gain an important insight that the difference in learned representation balancing patterns, measured by $Wass$ (or $\hat{d}_{\mathcal{H}}$), between DGNet and GNet (or DINet and INet), is negligible. This means that PPBR has no impact on the representation balancing task. However, PPBR can improve the predictive power of factual outcomes, reducing ϵ_F by $|1.07/1.12 - 1| = 4.5\%$ for GNet and $|1.07/1.08 - 1| = 0.9\%$ for INet. Such improvement is pronounced in counterfactual estimation, where ϵ_{CF} is reduced by $|3.08/3.55 - 1| = 13.2\%$ for GNet and $|2.95/3.47 - 1| = 15.0\%$ for INet. Benefiting from the advantage of PPBR, the treatment

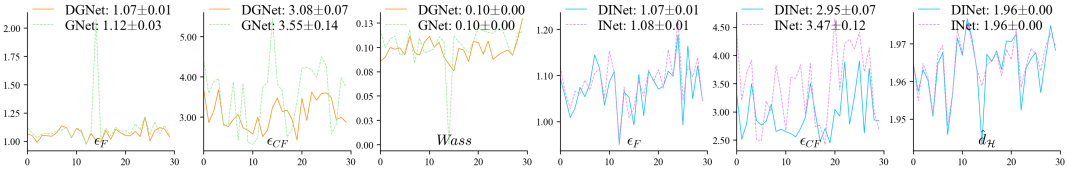

Figure 4: Plots of model performances on test set for ϵ_F, ϵ_{CF}, $\hat{d}_{\mathcal{H}}$, and $Wass$ when $\gamma = 3$. Left graphs compare DGNet with GNet, and right graphs compare DINet with INet. Each graph plots the metric for 30 runs. Mean $\pm$ std of each metric averaged across 30 runs are reported on the top.

Table 1: Training- & test- set ϵ_{PEHE} & ϵ_{ATE} when $\gamma = 3$. Mean $\pm$ standard error of 30 runs.

	Training set		Test set	
	ϵ_{PEHE}	ϵ_{ATE}	ϵ_{PEHE}	ϵ_{ATE}
GNet	3.30±0.15	2.58±0.14	3.30±0.16	2.59±0.14
INet	3.24±0.11	2.46±0.09	3.22±0.12	2.47±0.10
DGNet	2.86±0.06	2.15±0.03	2.83±0.07	2.15±0.04
DINet	2.70±0.06	2.12±0.04	2.69±0.08	2.13±0.05
DIGNet	2.66±0.07	2.04±0.05	2.63±0.07	2.03±0.04

Table 2: Training- & test- set ϵ_{PEHE} & ϵ_{ATE} on IHDP. Mean $\pm$ standard error of 100 runs.

	Training set		Test set	
	ϵ_{PEHE}	ϵ_{ATE}	ϵ_{PEHE}	ϵ_{ATE}
GNet	0.71±0.15	0.12±0.01	0.77±0.18	0.15±0.02
INet	0.66±0.09	0.13±0.01	0.72±0.11	0.15±0.02
DGNet	0.53±0.07	0.11±0.01	0.60±0.09	0.13±0.01
DINet	0.57±0.12	0.13±0.01	0.60±0.11	0.14±0.01
DIGNet	0.42±0.02	0.11±0.01	0.45±0.04	0.12±0.01

effect errors (ϵ_{PEHE} and ϵ_{ATE}) attained by DINet and DGNet are significantly smaller than those attained by INet and GNet, as shown in Table 1.

Comparisons on IHDP benchmark. We first conduct an ablation study for PDIG and PPBR on 1-100 IHDP datasets and report the results in Table 2. Further, we undergo comparisons between DIGNet and other causal models on 1-1000 IHDP datasets and report the results in Table 3. The results in Table 2 show that DINet and DGNet are superior to INet and GNet but inferior to DIGNet concerning treatment effect estimation, suggesting that each component of PDIG and PPBR is advantageous for treatment effect estimation. This is consistent with the findings presented in the simulation study. Moreover, the results displayed in Table 3 demonstrate that our model prominently outperforms the previous well-known neural network causal models and recent representation balancing models toward treatment effect estimation. Compared to the second best method, DIGNet reduces the errors in ϵ_{PEHE} and ϵ_{ATE} on test set by $|0.45/0.57 - 1| = 21\%$ and $|0.12/0.13 - 1| = 7.7\%$, respectively.

Table 3: Training- & test- set ϵ_{PEHE} & ϵ_{ATE} on IHDP. Mean $\pm$ standard error of 1000 runs.

	Training set		Test set	
	$\sqrt{\epsilon_{PEHE}}$	ϵ_{ATE}	$\sqrt{\epsilon_{PEHE}}$	ϵ_{ATE}
CEVAE (Louizos et al., 2017)	$2.7 \pm .1$	$.34 \pm .01$	$2.6 \pm .1$	$.46 \pm .02$
TARNet (Shalit et al., 2017)	$.88 \pm .0$	$.26 \pm .01$	$.95 \pm .0$	$.28 \pm .01$
SITE (Yao et al., 2018)	$.69 \pm .0$	$.22 \pm .01$	$.75 \pm .0$	$.24 \pm .01$
GANITE (Yoon et al., 2018)	$1.9 \pm .4$	$.43 \pm .05$	$2.4 \pm .4$	$.49 \pm .05$
Dragonnet (Shi et al., 2019)	$1.3 \pm .4$	$.14 \pm .01$	$1.3 \pm .5$	$.20 \pm .05$
BNN (Johansson et al., 2016)	$2.2 \pm .1$	$.37 \pm .03$	$2.1 \pm .1$	$.42 \pm .03$
CFR-Wass (GNet) (Shalit et al., 2017)	$.73 \pm .0$	$.12 \pm .01$	$.81 \pm .0$	$.15 \pm .01$
MBRL (Huang et al., 2022a)	$.52 \pm .0$	$.12 \pm .01$	$.57 \pm .0$	$.13 \pm .01$
DIGNet (Ours)	$\mathbf{.42 \pm .0}$	$\mathbf{.11 \pm .01}$	$\mathbf{.45 \pm .0}$	$\mathbf{.12 \pm .01}$

6 Conclusion

In this paper, we derive a theoretical ITE bound based on $\mathcal{H}$-divergence and connect representation balancing with the concept of propensity confusion. Furthermore, we propose the components of PDIG and PPBR, on which we construct a decomposition network structure DIGNet for treatment effect estimation. Comprehensive experiments verify that PDIG and PPBR follow different pathways to achieve the same goal of improving treatment effect estimation. In particular, PDIG helps the model better capture representation balancing patterns to improve counterfactual estimation, while PPBR preserves patterns predictive of outcomes to enhance the outcome prediction, especially counterfactual estimates. We hope that our findings constitute an important step towards the generalizability of representation balancing models in counterfactual estimation.

A promising direction for future work is to discourage redundancy of shared information of balancing patterns in the PDIG structure. In addition, it is also meaningful to advance the exploration of more factors that are constructive for treatment effect estimation from a theoretical perspective.

REFERENCES

Serge Assaad, Shuxi Zeng, Chenyang Tao, Shounak Datta, Nikhil Mehta, Ricardo Henao, Fan Li, and Lawrence Carin. Counterfactual representation learning with balancing weights. In *International Conference on Artificial Intelligence and Statistics*, pp. 1972–1980. PMLR, 2021.

Susan Athey and Stefan Wager. Estimating treatment effects with causal forests: An application. *Observational Studies*, 5(2):37–51, 2019.

Shai Ben-David, John Blitzer, Koby Crammer, and Fernando Pereira. Analysis of representations for domain adaptation. *Advances in neural information processing systems*, 19, 2006.

Shai Ben-David, John Blitzer, Koby Crammer, Alex Kulesza, Fernando Pereira, and Jennifer Wortman Vaughan. A theory of learning from different domains. *Machine learning*, 79(1):151–175, 2010.

Ioana Bica, Ahmed M Alaa, Craig Lambert, and Mihaela Van Der Schaar. From real-world patient data to individualized treatment effects using machine learning: current and future methods to address underlying challenges. *Clinical Pharmacology & Therapeutics*, 109(1):87–100, 2021a.

Ioana Bica, Daniel Jarrett, Alihan Hüyük, and Mihaela van der Schaar. Learning "what-if" explanations for sequential decision-making. In *International Conference on Learning Representations*, 2021b. URL `https://openreview.net/forum?id=h0de3QWtGG`.

Victor Chernozhukov, Denis Chetverikov, Mert Demirer, Esther Duflo, Christian Hansen, Whitney Newey, and James Robins. Double/debiased machine learning for treatment and structural parameters. *The Econometrics Journal*, 21(1):C1–C68, 2018.

Hugh A Chipman, Edward I George, and Robert E McCulloch. Bart: Bayesian additive regression trees. *The Annals of Applied Statistics*, 4(1):266–298, 2010.

Zhixuan Chu, Stephen L. Rathbun, and Sheng Li. Graph infomax adversarial learning for treatment effect estimation with networked observational data. In *KDD*, pp. 176–184, 2021. URL `https://doi.org/10.1145/3447548.3467302`.

Richard K Crump, V Joseph Hotz, Guido W Imbens, and Oscar A Mitnik. Nonparametric tests for treatment effect heterogeneity. *The Review of Economics and Statistics*, 90(3):389–405, 2008.

Alicia Curth and Mihaela van der Schaar. On inductive biases for heterogeneous treatment effect estimation. *Advances in Neural Information Processing Systems*, 34:15883–15894, 2021.

Marco Cuturi and Arnaud Doucet. Fast computation of wasserstein barycenters. In *International conference on machine learning*, pp. 685–693. PMLR, 2014.

Vincent Dorie. Nonparametric methods for causal inference. https://github.com/vdorie/npci, 2021.

Xin Du, Lei Sun, Wouter Duivesteijn, Alexander Nikolaev, and Mykola Pechenizkiy. Adversarial balancing-based representation learning for causal effect inference with observational data. *Data Mining and Knowledge Discovery*, 35(4):1713–1738, 2021.

Max H Farrell. Robust inference on average treatment effects with possibly more covariates than observations. *Journal of Econometrics*, 189(1):1–23, 2015.

Yaroslav Ganin, Evgeniya Ustinova, Hana Ajakan, Pascal Germain, Hugo Larochelle, François Laviolette, Mario Marchand, and Victor Lempitsky. Domain-adversarial training of neural networks. *The journal of machine learning research*, 17(1):2096–2030, 2016.

Ruocheng Guo, Lu Cheng, Jundong Li, P Richard Hahn, and Huan Liu. A survey of learning causality with data: Problems and methods. *ACM Computing Surveys (CSUR)*, 53(4):1–37, 2020a.

Ruocheng Guo, Jundong Li, Yichuan Li, K Selçuk Candan, Adrienne Raglin, and Huan Liu. Ignite: A minimax game toward learning individual treatment effects from networked observational data. In *IJCAI*, pp. 4534–4540, 2020b.

Ruocheng Guo, Jundong Li, and Huan Liu. Learning individual causal effects from networked observational data. In *Proceedings of the 13th International Conference on Web Search and Data Mining*, pp. 232–240, 2020c.

Negar Hassanpour and Russell Greiner. Counterfactual regression with importance sampling weights. In *IJCAI*, pp. 5880–5887, 2019a.

Negar Hassanpour and Russell Greiner. Learning disentangled representations for counterfactual regression. In *International Conference on Learning Representations*, 2019b.

Jennifer L Hill. Bayesian nonparametric modeling for causal inference. *Journal of Computational and Graphical Statistics*, 20(1):217–240, 2011.

Yiyan Huang, Cheuk Hang Leung, Xing Yan, Qi Wu, Nanbo Peng, Dongdong Wang, and Zhixiang Huang. The causal learning of retail delinquency. In *Proceedings of the AAAI Conference on Artificial Intelligence*, volume 35, pp. 204–212, 2021.

Yiyan Huang, Cheuk Hang Leung, Shumin Ma, Qi Wu, Dongdong Wang, and Zhixiang Huang. Moderately-balanced representation learning for treatment effects with orthogonality information. 2022a.

Yiyan Huang, Cheuk Hang Leung, Qi Wu, Xing Yan, Shumin Ma, Zhiri Yuan, Dongdong Wang, and Zhixiang Huang. Robust causal learning for the estimation of average treatment effects. In *2022 International Joint Conference on Neural Networks (IJCNN 2022)*. IEEE, 2022b.

Guido W Imbens and Jeffrey M Wooldridge. Recent developments in the econometrics of program evaluation. *Journal of economic literature*, 47(1):5–86, 2009.

Fredrik Johansson, Uri Shalit, and David Sontag. Learning representations for counterfactual inference. In *International conference on machine learning*, pp. 3020–3029. PMLR, 2016.

Fredrik D. Johansson, Uri Shalit, Nathan Kallus, and David Sontag. Generalization bounds and representation learning for estimation of potential outcomes and causal effects. *Journal of Machine Learning Research*, 23(166):1–50, 2022. URL `http://jmlr.org/papers/v23/19-511.html`.

Kun Kuang, Peng Cui, Bo Li, Meng Jiang, Shiqiang Yang, and Fei Wang. Treatment effect estimation with data-driven variable decomposition. In *Proceedings of the AAAI Conference on Artificial Intelligence*, volume 31, 2017.

Sören R Künzel, Jasjeet S Sekhon, Peter J Bickel, and Bin Yu. Metalearners for estimating heterogeneous treatment effects using machine learning. *Proceedings of the national academy of sciences*, 116(10):4156–4165, 2019.

Mingsheng Long, Jianmin Wang, Guiguang Ding, Jiaguang Sun, and Philip S Yu. Transfer joint matching for unsupervised domain adaptation. In *Proceedings of the IEEE conference on computer vision and pattern recognition*, pp. 1410–1417, 2014.

Christos Louizos, Uri Shalit, Joris M Mooij, David Sontag, Richard Zemel, and Max Welling. Causal effect inference with deep latent-variable models. *Advances in neural information processing systems*, 30, 2017.

Maggie Makar, Fredrik Johansson, John Guttag, and David Sontag. Estimation of bounds on potential outcomes for decision making. In *International Conference on Machine Learning*, pp. 6661–6671. PMLR, 2020.

Xinkun Nie and Stefan Wager. Quasi-oracle estimation of heterogeneous treatment effects. *Biometrika*, 108(2):299–319, 2021.

Zhaozhi Qian, Yao Zhang, Ioana Bica, Angela Wood, and Mihaela van der Schaar. Synctwin: Treatment effect estimation with longitudinal outcomes. *Advances in Neural Information Processing Systems*, 34:3178–3190, 2021.

Paul R Rosenbaum and Donald B Rubin. The central role of the propensity score in observational studies for causal effects. *Biometrika*, 70(1):41–55, 1983.

Donald B Rubin. Causal inference using potential outcomes: Design, modeling, decisions. *Journal of the American Statistical Association*, 100(469):322–331, 2005.

Shai Shalev-Shwartz and Shai Ben-David. *Understanding machine learning: From theory to algorithms*. Cambridge university press, 2014.

Uri Shalit, Fredrik D Johansson, and David Sontag. Estimating individual treatment effect: generalization bounds and algorithms. In *International Conference on Machine Learning*, pp. 3076–3085. PMLR, 2017.

Jian Shen, Yanru Qu, Weinan Zhang, and Yong Yu. Wasserstein distance guided representation learning for domain adaptation. In *Proceedings of the AAAI Conference on Artificial Intelligence*, volume 32, 2018.

Claudia Shi, David Blei, and Victor Veitch. Adapting neural networks for the estimation of treatment effects. *Advances in neural information processing systems*, 32, 2019.

Bharath K Sriperumbudur, Kenji Fukumizu, Arthur Gretton, Bernhard Schölkopf, and Gert RG Lanckriet. On the empirical estimation of integral probability metrics. *Electronic Journal of Statistics*, 6:1550–1599, 2012.

Stefan Wager and Susan Athey. Estimation and inference of heterogeneous treatment effects using random forests. *Journal of the American Statistical Association*, 113(523):1228–1242, 2018.

Liuyi Yao, Sheng Li, Yaliang Li, Mengdi Huai, Jing Gao, and Aidong Zhang. Representation learning for treatment effect estimation from observational data. *Advances in Neural Information Processing Systems*, 31, 2018.

Liuyi Yao, Zhixuan Chu, Sheng Li, Yaliang Li, Jing Gao, and Aidong Zhang. A survey on causal inference. *ACM Transactions on Knowledge Discovery from Data (TKDD)*, 15(5):1–46, 2021.

Jinsung Yoon, James Jordon, and Mihaela Van Der Schaar. Ganite: Estimation of individualized treatment effects using generative adversarial nets. In *International Conference on Learning Representations*, 2018.

Yao Zhang, Alexis Bellot, and Mihaela Schaar. Learning overlapping representations for the estimation of individualized treatment effects. In *International Conference on Artificial Intelligence and Statistics*, pp. 1005–1014. PMLR, 2020.

Guanglin Zhou, Lina Yao, Xiwei Xu, Chen Wang, and Liming Zhu. Cycle-balanced representation learning for counterfactual inference. In *Proceedings of the 2022 SIAM International Conference on Data Mining (SDM)*, pp. 442–450. SIAM, 2022.

A Appendix

A.1 Preliminaries

We start by making some assumptions about the distribution we concern, and give some necessary definitions and results. We agree with the strong ignorability assumption, which assume that there exists a joint distribution $p(\mathbf{X}, T, Y^0, Y^1)$ such that conditioning on covariate $\mathbf{X}$, the potential outcomes Y^0, Y^1 are independent of T, i.e., $(Y^0, Y^1) \perp\!\!\!\perp T \mid \mathbf{X}$, and the propensity score $e(\mathbf{x}) := p(T = 1 \mid \mathbf{X} = \mathbf{x})$ is bounded away from 0 to 1, i.e. $0 < e(\mathbf{x}) < 1$. Recall that we also assume consistency, i.e., if the treatment is t, the observed outcome equals Y^t. These assumptions are crucial conditions that make individual treatment effect identifiable (Imbens & Wooldridge, 2009).

Definition 1 *The individual treatment effect (ITE) for unit* $\mathbf{x}$ *is:*

$$\tau(\mathbf{x}) = \mathbb{E}\left[Y^1 - Y^0 \mid \mathbf{X} = \mathbf{x}\right].$$

Let $\tau^t(\mathbf{x}) := \mathbb{E}[Y^t \mid \mathbf{X} = \mathbf{x}]$, we have $\tau(\mathbf{x}) = \tau^1(\mathbf{x}) - \tau^0(\mathbf{x})$. Let $f : \mathcal{X} \times \{0,1\} \to \mathcal{Y}$ be a prediction function.

Definition 2 *The individual treatment effect estimate can be defined as:*

$$\hat{\tau}_f(\mathbf{x}) := f(\mathbf{x}, 1) - f(\mathbf{x}, 0).$$

Definition 3 *(Hill, 2011) Let $L : \mathcal{Y} \times \mathcal{Y} \to \mathbb{R}_+$ be a loss function. The expected Precision in Estimation of Heterogeneous Effect (PEHE) loss of f is:*

$$\epsilon_{PEHE}(f) = \int_{\mathcal{X}} L(\hat{\tau}_f(\mathbf{x}) - \tau(\mathbf{x}))p(\mathbf{x})d\mathbf{x}.$$

Definition 4 *The covariates' distributions in the treated and controlled groups can be denoted by $p^{T=1}(\mathbf{x}) := p(\mathbf{x} \mid T = 1)$ and $p^{T=0}(\mathbf{x}) := p(\mathbf{x} \mid T = 0)$, respectively.*

In our causal representation balancing approach, we assume that the representation function $\Phi : \mathcal{X} \to \mathcal{R}$ is a twice-differentiable, one-to-one function, where $\mathcal{R} \subset \mathbb{R}^d$ is the representation space. Then, we can denote $\Psi : \mathcal{R} \to \mathcal{X}$ by the inverse of Φ and the induced distribution of $\mathbf{r}$ by p_Φ.

Definition 5 *The covariates' distributions in the treated and controlled groups over $\mathcal{R}$ can be denoted by $p_\Phi^{T=1}(\mathbf{r}) := p_\Phi(\mathbf{r} \mid T = 1)$ and $p_\Phi^{T=0}(\mathbf{r}) := p_\Phi(\mathbf{r} \mid T = 0)$, respectively.*

Let $h : \mathcal{R} \times \{0,1\} \to \mathcal{Y}$ be an hypothesis defined over the representation space $\mathcal{R}$, such that $f(\mathbf{x}, t) = h(\Phi(\mathbf{x}), t)$.

Definition 6 *The expected loss for the unit and treatment pair $(\mathbf{x}, t)$ is :*

$$\ell_{h,\Phi}(\mathbf{x}, t) = \int_{\mathcal{Y}} L(y^t, h(\Phi(\mathbf{x}), t))p(y^t|\mathbf{x})dy^t.$$

Definition 7 *The expected factual loss and counterfactual losses of h and Φ are, respectively:*

$$\epsilon_F(h, \Phi) = \int_{\mathcal{X}\times\{0,1\}} \ell_{h,\Phi}(\mathbf{x}, t)p(\mathbf{x}, t)d\mathbf{x}dt,$$
$$\epsilon_{CF}(h, \Phi) = \int_{\mathcal{X}\times\{0,1\}} \ell_{h,\Phi}(\mathbf{x}, t)p(\mathbf{x}, 1-t)d\mathbf{x}dt.$$

Definition 8 *The expected treated and control losses are:*

$$\epsilon_F^{T=1}(h, \Phi) = \int_{\mathcal{X}} \ell_{h,\Phi}(\mathbf{x}, 1)p^{T=1}(\mathbf{x})d\mathbf{x},$$
$$\epsilon_F^{T=0}(h, \Phi) = \int_{\mathcal{X}} \ell_{h,\Phi}(\mathbf{x}, 0)p^{T=0}(\mathbf{x})d\mathbf{x},$$
$$\epsilon_{CF}^{T=1}(h, \Phi) = \int_{\mathcal{X}} \ell_{h,\Phi}(\mathbf{x}, 1)p^{T=0}(\mathbf{x})d\mathbf{x},$$
$$\epsilon_{CF}^{T=0}(h, \Phi) = \int_{\mathcal{X}} \ell_{h,\Phi}(\mathbf{x}, 0)p^{T=1}(\mathbf{x})d\mathbf{x}.$$

Let $u := Pr(T = 1)$ be the proportion of treated in the population. We then have the result:

Lemma 1

$$\epsilon_F(h, \Phi) = u \cdot \epsilon_F^{T=1}(h, \Phi) + (1-u) \cdot \epsilon_F^{T=0}(h, \Phi),$$
$$\epsilon_{CF}(h, \Phi) = (1-u) \cdot \epsilon_{CF}^{T=1}(h, \Phi) + u \cdot \epsilon_{CF}^{T=0}(h, \Phi).$$

Noting that $p(\mathbf{x}, t) = u \cdot p^{T=1}(\mathbf{x}) + (1-u) \cdot p^{T=0}(\mathbf{x})$, the results can be easily obtained from the Definitions 7 and 8.

Definition 9 *Let $\mathcal{G}$ be a function family consisting of functions $g : \mathcal{S} \to \mathbb{R}$. For a pair of distributions p_1, p_2 over $\mathcal{S}$, define the Integral Probability Metric:*

$$IPM_{\mathcal{G}}(p_1, p_2) = \sup_{g\in\mathcal{G}} |\int_{\mathcal{S}} g(s)(p_1(s) - p_2(s))ds|.$$

Let $\mathcal{G}$ be the family of 1-Lipschitz functions, we obtain the so-called 1-Wasserstein distance between distributions, which we denote $Wass(p_1, p_2)$ (Sriperumbudur et al., 2012).

Definition 10 *Given a pair of distributions p_1, p_2 over $\mathcal{S}$, and a hypothesis binary function class $\mathcal{H}$, the $\mathcal{H}$-divergence between p_1 and p_2 is*

$$d_{\mathcal{H}}(p_1, p_2) = 2sup_{\eta \in \mathcal{H}} \left| Pr_{p_1}[\eta(s) = 1] - Pr_{p_2}[\eta(s) = 1] \right|.$$

Lemma 2 *Let $\mathcal{G}$ in Definition 9 be the family of binary functions, we obtain half of $\mathcal{H}$-divergence.*

Proof *Let $\mathbb{I}(\cdot)$ denotes an indicator function.*

$$\begin{aligned}
&d_{\mathcal{H}}(p_1, p_2) \\
=&2 \sup_{\eta \in \mathcal{H}} \left| \int_{\eta(s)=1} (p_1(s) - p_2(s)) ds \right| \\
=&2 \sup_{\eta \in \mathcal{H}} \left| \int_{\mathcal{S}} \mathbb{I}(\eta(s) = 1)(p_1(s) - p_2(s)) ds \right| \\
=&2 \sup_{\eta \in \mathcal{H}} \left| \int_{\mathcal{S}} \eta(s)(p_1(s) - p_2(s)) ds \right|
\end{aligned} \tag{18}$$

The last equation is because an indicator function is also a binary function.

□

A.2 Bounds for conterfactual error ϵ_{CF}

We first derive the counterfactual error bounds when using Wasserstein distance. The following Lemma 3 and corresponding proof is identical to the Lemma 1 in (Shalit et al., 2017).

Lemma 3 *Let $\Phi : \mathcal{X} \to \mathcal{R}$ be an invertible representation with Ψ being its inverse. Let $p_\Phi^{T=1}(\mathbf{r})$, $p_\Phi^{T=0}(\mathbf{r})$ be as defined before. Let $h : \mathcal{R} \times \{0, 1\} \to \mathcal{Y}$, $u := Pr(T = 1)$ and $\mathcal{G}$ be the family of 1-Lipschitz functions. Assume there exists a constant $B_\Phi \geq 0$, such that for $t = 0, 1$, the function $g_{\Phi,h}(\mathbf{r}, t) := \frac{1}{B_\Phi} \cdot \ell_{h,\Phi}(\Psi(\mathbf{r}), t) \in \mathcal{G}$. Then we have:*

$$\epsilon_{CF}(h, \Phi) \leq (1 - u) \cdot \epsilon_F^{T=1}(h, \Phi) + u \cdot \epsilon_F^{T=0}(h, \Phi) + B_\Phi \cdot Wass(p_\Phi^{T=1}, p_\Phi^{T=0}).$$

Proof

$$\begin{aligned}
&\epsilon_{CF}(h, \Phi) - [(1 - u) \cdot \epsilon_F^{T=1}(h, \Phi) + u \cdot \epsilon_F^{T=0}(h, \Phi)] \\
=&[(1 - u) \cdot \epsilon_{CF}^{T=1}(h, \Phi) + u \cdot \epsilon_{CF}^{T=0}(h, \Phi)] - [(1 - u) \cdot \epsilon_F^{T=1}(h, \Phi) + u \cdot \epsilon_F^{T=0}(h, \Phi)] \\
=&(1 - u) \cdot [\epsilon_{CF}^{T=1}(h, \Phi) - \epsilon_F^{T=1}(h, \Phi)] + u \cdot [\epsilon_{CF}^{T=0}(h, \Phi) - \epsilon_F^{T=0}(h, \Phi)] \\
=&(1 - u) \int_{\mathcal{X}} \ell_{h,\Phi}(\mathbf{x}, 1)(p^{T=0}(\mathbf{x}) - p^{T=1}(\mathbf{x})) d\mathbf{x} + u \int_{\mathcal{X}} \ell_{h,\Phi}(\mathbf{x}, 0)(p^{T=1}(\mathbf{x}) - p^{T=0}(\mathbf{x})) d\mathbf{x}
\end{aligned} \tag{19}$$

$$=(1 - u) \int_{\mathcal{R}} \ell_{h,\Phi}(\Psi(\mathbf{r}), 1)(p_\Phi^{T=0}(\mathbf{r}) - p_\Phi^{T=1}(\mathbf{r})) d\mathbf{r} + u \int_{\mathcal{R}} \ell_{h,\Phi}(\Psi(\mathbf{r}), 0)(p_\Phi^{T=1}(\mathbf{r}) - p_\Phi^{T=0}(\mathbf{r})) d\mathbf{r} \tag{20}$$

$$\begin{aligned}
\leq&B_\Phi \cdot (1 - u) \int_{\mathcal{R}} \frac{1}{B_\Phi} \ell_{h,\Phi}(\Psi(\mathbf{r}), 1)(p_\Phi^{T=0}(\mathbf{r}) - p_\Phi^{T=1}(\mathbf{r})) d\mathbf{r} \\
&+ B_\Phi \cdot u \int_{\mathcal{R}} \frac{1}{B_\Phi} \ell_{h,\Phi}(\Psi(\mathbf{r}), 0)(p_\Phi^{T=1}(\mathbf{r}) - p_\Phi^{T=0}(\mathbf{r})) d\mathbf{r} \\
\leq&B_\Phi \cdot (1 - u) \sup_{g \in \mathcal{G}} \left| \int_{\mathcal{R}} g(\mathbf{r})(p_\Phi^{T=0}(\mathbf{r}) - p_\Phi^{T=1}(\mathbf{r})) d\mathbf{r} \right| \\
&+ B_\Phi \cdot u \cdot \sup_{g \in \mathcal{G}} \left| \int_{\mathcal{R}} g(\mathbf{r})(p_\Phi^{T=1}(\mathbf{r}) - p_\Phi^{T=0}(\mathbf{r})) d\mathbf{r} \right|
\end{aligned} \tag{21}$$

$$=B_\Phi \cdot Wass(p_\Phi^{T=1}, p_\Phi^{T=0}) \tag{22}$$

Equation (19) is by Definition 8; equation (20) is by the change of formula, $p_\Phi^{T=0}(\mathbf{r}) = p^{T=0}(\Psi(\mathbf{r}))J_\Psi(\mathbf{r})$, $p_\Phi^{T=1}(\mathbf{r}) = p^{T=1}(\Psi(\mathbf{r}))J_\Psi(\mathbf{r})$, *where* $J_\Psi(\mathbf{r})$ *is the absolute of the determinant of the Jacobian of* $\Psi(\mathbf{r})$*; inequality (21) is by the premise that* $\frac{1}{B_\Phi} \cdot \ell_{h,\Phi}(\Psi(\mathbf{r}), t) \in \mathcal{G}$ *for* $t = 0, 1$*, and (22) is by Definition 9 of an IPM.* □

The crucial condition in Lemma 3 is that $g_{\Phi,h}(\mathbf{r}, t) := \frac{1}{B_\Phi} \cdot \ell_{h,\Phi}(\Psi(\mathbf{r}), t) \in \mathcal{G}$. Bounds for B_Φ can be given to evaluate this constant when under more assumptions about the loss function L, the Lipschitz constants of $p(y^t|\mathbf{x})$, h, and the condition number of the Jacobian of Φ. These assumptions and the specific bounds for B_Φ can be seen in supplement Section A.3 of (Shalit et al., 2017).

Now we turn to derive the counterfactual error bounds for the $\mathcal{H}$-divergence case.

Assumption 1 *There exists a constant* K *such that for all* $y_2 \in \mathcal{Y}$, $\int_{\mathcal{Y}} L(y_1, y_2)dy_1 \leq K$.

Lemma 4 *Let* $\Phi : \mathcal{X} \to \mathcal{R}$ *be an invertible representation with* Ψ *being its inverse. Let* $p_\Phi^{T=1}(\mathbf{r})$, $p_\Phi^{T=0}(\mathbf{r})$ *be as defined before. Let* $h : \mathcal{R} \times \{0, 1\} \to \mathcal{Y}$, $u := Pr(T = 1)$ *and* $\mathcal{H}$ *be the family of binary functions. Assume loss function* L *obeys the Assumption 1. Then we have:*

$$\epsilon_{CF}(h, \Phi) \leq (1 - u) \cdot \epsilon_F^{T=1}(h, \Phi) + u \cdot \epsilon_F^{T=0}(h, \Phi) + \frac{K}{2} d_{\mathcal{H}}(p_\Phi^{T=1}, p_\Phi^{T=0}).$$

Proof

$$\begin{aligned}
&\epsilon_{CF}(h, \Phi) - [(1 - u) \cdot \epsilon_F^{T=1}(h, \Phi) + u \cdot \epsilon_F^{T=0}(h, \Phi)] \\
=&(1 - u) \int_{\mathcal{R}} \ell_{h,\Phi}(\Psi(\mathbf{r}), 1)(p_\Phi^{T=0}(\mathbf{r}) - p_\Phi^{T=1}(\mathbf{r}))d\mathbf{r} + u \int_{\mathcal{R}} \ell_{h,\Phi}(\Psi(\mathbf{r}), 0)(p_\Phi^{T=1}(\mathbf{r}) - p_\Phi^{T=0}(\mathbf{r}))d\mathbf{r} && (23)\\
\leq&(1 - u) \int_{p_\Phi^{T=0} > p_\Phi^{T=1}} \ell_{h,\Phi}(\Psi(\mathbf{r}), 1)(p_\Phi^{T=0}(\mathbf{r}) - p_\Phi^{T=1}(\mathbf{r}))d\mathbf{r} \\
&+ u \int_{p_\Phi^{T=1} > p_\Phi^{T=0}} \ell_{h,\Phi}(\Psi(\mathbf{r}), 0)(p_\Phi^{T=1}(\mathbf{r}) - p_\Phi^{T=0}(\mathbf{r}))d\mathbf{r} && (24)\\
\leq&(1 - u)K \int_{p_\Phi^{T=0} > p_\Phi^{T=1}} (p_\Phi^{T=0}(\mathbf{r}) - p_\Phi^{T=1}(\mathbf{r}))d\mathbf{r} + u \cdot K \int_{p_\Phi^{T=1} > p_\Phi^{T=0}} (p_\Phi^{T=1}(\mathbf{r}) - p_\Phi^{T=0}(\mathbf{r}))d\mathbf{r} && (25)\\
=&(1 - u)K \int_{\mathcal{R}} \mathbb{I}(p_\Phi^{t=0} > p_\Phi^{T=1})(p_\Phi^{T=0}(\mathbf{r}) - p_\Phi^{T=1}(\mathbf{r}))d\mathbf{r} \\
&+ u \cdot K \int_{\mathcal{R}} \mathbb{I}(p_\Phi^{T=1} > p_\Phi^{T=0})(p_\Phi^{T=1}(\mathbf{r}) - p_\Phi^{T=0}(\mathbf{r}))d\mathbf{r} \\
\leq&(1 - u)K \sup_{\eta \in \mathcal{H}} |\int_{\mathcal{R}} \eta(\mathbf{r})(p_\Phi^{T=1}(\mathbf{r}) - p_\Phi^{T=0}(\mathbf{r}))d\mathbf{r}| \\
&+ u \cdot K \cdot \sup_{\eta \in \mathcal{H}} |\int_{\mathcal{R}} \eta(\mathbf{r})(p_\Phi^{T=1}(\mathbf{r}) - p_\Phi^{T=0}(\mathbf{r}))d\mathbf{r}| && (26)\\
\leq&K \cdot \sup_{\eta \in \mathcal{H}} |\int_{\mathcal{R}} \eta(\mathbf{r})((p_\Phi^{T=1}(\mathbf{r}) - p_\Phi^{T=0}(\mathbf{r})))d\mathbf{r}| \\
=&\frac{K}{2} d_{\mathcal{H}}(p_\Phi^{T=1}, p_\Phi^{T=0}) && (27)
\end{aligned}$$

Equation (23) is same to equation (20); equation (24) is by $\ell_{h,\Phi} \geq 0$ *for all* $\mathbf{r}$ *and* t*; inequality (25) is by Definition 6 and Assumption 1; inequality (26) is because an indicator function is also a binary function; equation (27) is by (18) in Lemma 2.* □

A.3 Bounds for the PEHE loss ϵ_{PEHE}

We first state two lemmas for ϵ_{PEHE} with respect to two different loss functions: the squared loss and the absolute loss. In fact, similar lemmas hold for loss functions that satisfy the (relaxed) triangle inequalities.

Definition 11 *The expected variance of y^t with regard to $p(\mathbf{x}, t)$ is:*

$$\sigma^2_{y^t}(p(\mathbf{x}, t)) = \int_{\mathcal{X}\times\{0,1\}\times\mathcal{Y}} (y^t - \tau^t(\mathbf{x}))^2 p(y^t|\mathbf{x})p(\mathbf{x}, t)dy^t d\mathbf{x}dt,$$

and define:

$$\sigma^2_y = \min\{\sigma^2_{y^t}(p(\mathbf{x}, t)), \sigma^2_{y^t}(p(\mathbf{x}, 1-t))\}.$$

Lemma 5 *Let loss function L be the squared loss, $L(y_1, y_2) = (y_1 - y_2)^2$. For any function $f : \mathcal{X} \times \{0, 1\} \to \mathcal{Y}$, and distribution $p(\mathbf{x}, t)$ over $\mathcal{X} \times \{0, 1\}$:*

$$\epsilon_{PEHE}(h, \Phi) \leq 2(\epsilon_{CF}(h, \Phi) + \epsilon_F(h, \Phi) - 2\sigma^2_y)$$

Proof *We denote $\epsilon_{PEHE}(f) = \epsilon_{PEHE}(h, \Phi)$, $\epsilon_F(f) = \epsilon_F(h, \Phi)$, $\epsilon_{CF}(f) = \epsilon_{CF}(h, \Phi)$ for $f(\mathbf{x}, t) = h(\Phi(\mathbf{x}), t)$.*

$$\begin{aligned}
&\epsilon_{PEHE}(f)\\
=&\int_{\mathcal{X}} ((f(\mathbf{x}, 1) - f(\mathbf{x}, 0)) - (\tau^1(\mathbf{x}) - \tau^0(\mathbf{x})))^2 p(\mathbf{x})d\mathbf{x}\\
\leq& 2\int_{\mathcal{X}} ((f(\mathbf{x}, 1) - \tau^1(\mathbf{x}))^2 + (f(\mathbf{x}, 0) - \tau^0(\mathbf{x}))^2)p(\mathbf{x})d\mathbf{x} \qquad (28)\\
=&2\int_{\mathcal{X}} (f(\mathbf{x}, 1) - \tau^1(\mathbf{x}))^2 p(\mathbf{x}, T = 1)d\mathbf{x} + 2\int_{\mathcal{X}} (f(\mathbf{x}, 0) - \tau^0(\mathbf{x}))^2 p(\mathbf{x}, T = 0)d\mathbf{x}\\
&+ 2\int_{\mathcal{X}} (f(\mathbf{x}, 1) - \tau^1(\mathbf{x}))^2 p(\mathbf{x}, T = 0)d\mathbf{x} + 2\int_{\mathcal{X}} (f(\mathbf{x}, 0) - \tau^0(\mathbf{x}))^2 p(\mathbf{x}, T = 1)d\mathbf{x} \qquad (29)\\
=&2\int_{\mathcal{X}\times\{0,1\}} (f(\mathbf{x}, t) - \tau^t(\mathbf{x}))^2 p(\mathbf{x}, t)d\mathbf{x}dt + 2\int_{\mathcal{X}\times\{0,1\}} (f(\mathbf{x}, t) - \tau^t(\mathbf{x}))^2 p(\mathbf{x}, 1-t)d\mathbf{x}dt.
\end{aligned}$$

Inequality (28) is because the relaxed triangle inequality, $(x + y)^2 \leq 2(x^2 + y^2)$; equation (29) is because $p(\mathbf{x}) = p(\mathbf{x}, T = 0) + p(\mathbf{x}, T = 1)$.

$$\begin{aligned}
&\epsilon_F(f)\\
=&\int_{\mathcal{X}\times\{0,1\}\times\mathcal{Y}} (f(\mathbf{x}, t) - y^t)^2 p(y^t|\mathbf{x})p(\mathbf{x}, t)dy^t d\mathbf{x}dt\\
=&\int_{\mathcal{X}\times\{0,1\}\times\mathcal{Y}} (f(\mathbf{x}, t) - \tau^t(\mathbf{x}))^2 p(y^t|\mathbf{x})p(\mathbf{x}, t)dy^t d\mathbf{x}dt\\
&+ \int_{\mathcal{X}\times\{0,1\}\times\mathcal{Y}} (\tau^t(\mathbf{x}) - y^t)^2 p(y^t|\mathbf{x})p(\mathbf{x}, t)dy^t d\mathbf{x}dt\\
&+ 2\int_{\mathcal{X}\times\{0,1\}\times\mathcal{Y}} (f(\mathbf{x}, t) - \tau^t(\mathbf{x}))(\tau^t(\mathbf{x}) - y^t)p(y^t|\mathbf{x})p(\mathbf{x}, t)dy^t d\mathbf{x}dt \qquad (30)\\
=&\int_{\mathcal{X}\times\{0,1\}} (f(\mathbf{x}, t) - \tau^t(\mathbf{x}))^2 p(\mathbf{x}, t)d\mathbf{x}dt + \sigma^2_{y^t}(p(\mathbf{x}, t)) \qquad (31)
\end{aligned}$$

Equation (31) is by Definition 11 and last term in equation (30) equals to zero, since $\tau^t(\mathbf{x}) = \int_{\mathcal{Y}} y^t p(y^t|\mathbf{x})dy_t$. A similar result can be obtained for ϵ_{CF}:

$$\epsilon_{CF}(f) = \int_{\mathcal{X}\times\{0,1\}} (f(\mathbf{x}, t) - \tau^t(\mathbf{x}))^2 p(\mathbf{x}, 1-t)d\mathbf{x}dt + \sigma^2_{y^t}(p(\mathbf{x}, 1-t)).$$

Combining these results and Definition 11, we have

$$\begin{aligned}
\epsilon_{PEHE}(h, \Phi) &\leq 2(\epsilon_F(f) - \sigma^2_{y^t}(p(\mathbf{x}, t))) + 2(\epsilon_{CF}(f) - \sigma^2_{y^t}(p(\mathbf{x}, 1-t)))\\
&\leq 2(\epsilon_{CF}(h, \Phi) + \epsilon_F(h, \Phi) - 2\sigma^2_y).
\end{aligned}$$

□

For the absolute loss $L(y_1, y_2) = |y_1 - y_2|$ that satisfies triangle inequality, the upper bound in Lemma 5 will replace the standard deviation σ_y^2 by mean absolute deviation A_y.

Definition 12 *The mean absolute deviation of y^t with regard to $p(\mathbf{x}, t)$ is:*

$$A_{y^t}(p(\mathbf{x}, t)) = \int_{\mathcal{X}\times\{0,1\}\times\mathcal{Y}} |y^t - \tau^t(\mathbf{x})| p(y^t|\mathbf{x}) p(\mathbf{x}, t) dy^t d\mathbf{x} dt,$$

and define:

$$A_y = \min\{A_{y^t}(p(\mathbf{x}, t)), A_{y^t}(p(\mathbf{x}, 1-t))\}.$$

Lemma 6 *Let loss function L be the absolute loss, $L(y_1, y_2) = |y_1 - y_2|$. For any function $f : \mathcal{X} \times \{0, 1\} \to \mathcal{Y}$, and distribution $p(\mathbf{x}, t)$ over $\mathcal{X} \times \{0, 1\}$:*

$$\epsilon_{PEHE}(h, \Phi) \leq \epsilon_{CF}(h, \Phi) + \epsilon_F(h, \Phi) - 2A_y.$$

Proof *Recall that $\epsilon_{PEHE}(f) = \epsilon_{PEHE}(h, \Phi)$, $\epsilon_F(f) = \epsilon_F(h, \Phi)$, $\epsilon_{CF}(f) = \epsilon_{CF}(h, \Phi)$ for $f(\mathbf{x}, t) = h(\Phi(\mathbf{x}), t)$.*

$$\begin{aligned}
&\epsilon_{PEHE}(f) \\
&= \int_{\mathcal{X}} |(f(\mathbf{x}, 1) - f(\mathbf{x}, 0)) - (\tau^1(\mathbf{x}) - \tau^0(\mathbf{x}))| p(\mathbf{x}) d\mathbf{x} \\
&\leq \int_{\mathcal{X}} (|f(\mathbf{x}, 1) - \tau^1(\mathbf{x})| + |f(\mathbf{x}, 0) - \tau^0(\mathbf{x})|) p(\mathbf{x}) d\mathbf{x} \qquad (32) \\
&= \int_{\mathcal{X}} |f(\mathbf{x}, 1) - \tau^1(\mathbf{x})| p(\mathbf{x}, T = 1) d\mathbf{x} + \int_{\mathcal{X}} |f(\mathbf{x}, 0) - \tau^0(\mathbf{x})| p(\mathbf{x}, T = 0) d\mathbf{x} \\
&\quad + \int_{\mathcal{X}} |f(\mathbf{x}, 1) - \tau^1(\mathbf{x})| p(\mathbf{x}, T = 0) d\mathbf{x} + \int_{\mathcal{X}} |f(\mathbf{x}, 0) - \tau^0(\mathbf{x})| p(\mathbf{x}, T = 1) d\mathbf{x} \qquad (33) \\
&= \int_{\mathcal{X}\times\{0,1\}} |f(\mathbf{x}, t) - \tau^t(\mathbf{x})| p(\mathbf{x}, t) d\mathbf{x} dt + \int_{\mathcal{X}\times\{0,1\}} |f(\mathbf{x}, t) - \tau^t(\mathbf{x})| p(\mathbf{x}, 1-t) d\mathbf{x} dt.
\end{aligned}$$

Inequality (32) is because triangle inequality, $|x + y| \leq |x| + |y|$; equation (33) is because $p(\mathbf{x}) = p(\mathbf{x}, T = 0) + p(\mathbf{x}, T = 1)$.

$$\begin{aligned}
&\epsilon_F(f) \\
&= \int_{\mathcal{X}\times\{0,1\}\times\mathcal{Y}} |f(\mathbf{x}, t) - y^t| p(y^t|\mathbf{x}) p(\mathbf{x}, t) dy^t d\mathbf{x} dt \\
&\leq \int_{\mathcal{X}\times\{0,1\}\times\mathcal{Y}} |f(\mathbf{x}, t) - \tau^t(\mathbf{x})| p(y^t|\mathbf{x}) p(\mathbf{x}, t) dy^t d\mathbf{x} dt \\
&\quad + \int_{\mathcal{X}\times\{0,1\}\times\mathcal{Y}} |\tau^t(\mathbf{x}) - y^t| p(y^t|\mathbf{x}) p(\mathbf{x}, t) dy^t d\mathbf{x} dt \qquad (34) \\
&= \int_{\mathcal{X}\times\{0,1\}} |f(\mathbf{x}, t) - \tau^t(\mathbf{x})| p(\mathbf{x}, t) d\mathbf{x} dt + A_{y^t}(p(\mathbf{x}, t)). \qquad (35)
\end{aligned}$$

Inequality (34) is also because $|x+y| \leq |x|+|y|$, equation (35) is by Definition 12. A similar result can be obtained for ϵ_{CF}:

$$\epsilon_{CF}(f) = \int_{\mathcal{X}\times\{0,1\}} |f(\mathbf{x}, t) - \tau^t(\mathbf{x})| p(\mathbf{x}, 1-t) d\mathbf{x} dt + A_{y^t}(p(\mathbf{x}, 1-t)).$$

Combining these results and Definition 12, we have

$$\begin{aligned}
\epsilon_{PEHE}(h, \Phi) &\leq \epsilon_F(f) - A_{y^t}(p(\mathbf{x}, t)) + \epsilon_{CF}(f) - A_{y^t}(p(\mathbf{x}, 1-t)) \\
&\leq \epsilon_{CF}(h, \Phi) + \epsilon_F(h, \Phi) - 2A_y.
\end{aligned}$$

□

We summarize the upper bounds of ϵ_{CF} and ϵ_{PEHE} above, and give the final bounds for these two distance using the squared and absolute loss, respectively.

Theorem 3 *Let $\Phi : \mathcal{X} \to \mathcal{R}$ be an invertible representation with Ψ being its inverse. Let $p_\Phi^{T=1}(\mathbf{r})$, $p_\Phi^{T=0}(\mathbf{r})$ be as defined before. Let $h : \mathcal{R} \times \{0,1\} \to \mathcal{Y}$, $u := Pr(T=1)$ and $\mathcal{G}$ be the family of 1-Lipschitz functions. Assume there exists a constant $B_\Phi \geq 0$, such that for $t = 0, 1$, the function $g_{\Phi,h}(\mathbf{r}, t) := \frac{1}{B_\Phi} \cdot \ell_{h,\Phi}(\Psi(\mathbf{r}), t) \in \mathcal{G}$.*

Let loss function L be the squared loss, $L(y_1, y_2) = (y_1 - y_2)^2$.Then we have:

$$\begin{aligned}
&\epsilon_{PEHE}(h, \Phi) \\
\leq &2(\epsilon_{CF}(h, \Phi) + \epsilon_F(h, \Phi) - 2\sigma_y^2) && (36)\\
\leq &2(\epsilon_F^{T=1}(h, \Phi) + \epsilon_F^{T=0}(h, \Phi) + B_\Phi \cdot Wass(p_\Phi^{T=1}, p_\Phi^{T=0}) - 2\sigma_y^2) && (37)
\end{aligned}$$

Let loss function L be the absolute loss, $L(y_1, y_2) = |y_1 - y_2|$. Then we have:

$$\begin{aligned}
&\epsilon_{PEHE}(h, \Phi) \\
\leq &\epsilon_{CF}(h, \Phi) + \epsilon_F(h, \Phi) - 2A_y && (38)\\
\leq &\epsilon_F^{T=1}(h, \Phi) + \epsilon_F^{T=0}(h, \Phi) + B_\Phi \cdot Wass(p_\Phi^{T=1}, p_\Phi^{T=0}) - 2A_y && (39)
\end{aligned}$$

Proof *Inequality (36) is by Lemma 5, inequality (37) is by Lemma 1 and Lemma 3; Inequality (38) is by Lemma 6, inequality (39) is by Lemma 1 and Lemma 3;* □

Theorem 4 *Let $\Phi : \mathcal{X} \to \mathcal{R}$ be an invertible representation with Ψ being its inverse. Let $p_\Phi^{T=1}(\mathbf{r})$, $p_\Phi^{T=0}(\mathbf{r})$ be as defined before. Let $h : \mathcal{R} \times \{0,1\} \to \mathcal{Y}$, $u := Pr(T=1)$ and $\mathcal{H}$ be the family of binary functions.*

Let loss function L be the squared loss such that $L(y_1, y_2) = (y_1 - y_2)^2$. Then we have:

$$\begin{aligned}
&\epsilon_{PEHE}(h, \Phi) \\
\leq &2(\epsilon_{CF}(h, \Phi) + \epsilon_F(h, \Phi) - 2\sigma_y^2) && (40)\\
\leq &2(\epsilon_F^{T=1}(h, \Phi) + \epsilon_F^{T=0}(h, \Phi) + \frac{K}{2} d_{\mathcal{H}}(p_\Phi^{T=1}, p_\Phi^{T=0}) - 2\sigma_y^2) && (41)
\end{aligned}$$

Let loss function L be the absolute loss such that $L(y_1, y_2) = |y_1 - y_2|$. Then we have:

$$\begin{aligned}
&\epsilon_{PEHE}(h, \Phi) \\
\leq &\epsilon_{CF}(h, \Phi) + \epsilon_F(h, \Phi) - 2A_y && (42)\\
\leq &\epsilon_F^{T=1}(h, \Phi) + \epsilon_F^{T=0}(h, \Phi) + \frac{K}{2} d_{\mathcal{H}}(p_\Phi^{T=1}, p_\Phi^{T=0}) - 2A_y && (43)
\end{aligned}$$

Proof *Inequality (40) is by Lemma 5, inequality (41) is by Lemma 1 and Lemma 4; Inequality (42) is by Lemma 6, inequality (43) is by Lemma 1 and Lemma 4;* □

Obviously, when using Wasserstein distance, there are various versions of bounds for different loss functions as long as they satisfy the (relaxed) triangle inequality and assumptions about $\ell_{h,\Phi}$ in Theorem 3. Similarly, when using $\mathcal{H}$-divergence, there are also various versions of bounds for loss functions that satisfy Assumption 1 and the (relaxed) triangle inequality.

For an empirical sample and a family of representations and hypotheses, we can further upper bound $\epsilon_F^{T=0}$ and $\epsilon_F^{T=1}$ by their respective empirical losses and a model complexity term using standard arguments (Shalev-Shwartz & Ben-David, 2014). Both the Wasserstein distance and $\mathcal{H}$-divergence can be consistently estimated from finite samples (Sriperumbudur et al., 2012; Ben-David et al., 2006; 2010).

A.4 Additional Experimental details

Hyperparameters. In simulation studies, we ensure a fair comparison by fixing all the hyperparameters in all datasets across different models. The relevant details are stated in Table 4. In IHDP studies, to compare with the baseline model CFR-Wass (GNet), we remain the hyperparameters of INet, DGNet, DINet and the early stopping rule the same as those used in CFR-Wass Shalit et al. (2017). Since DIGNet is more complex than other four models, we adjust the hyperparameters of Φ_E, Φ_G, Φ_I, α_1, and α_2 for DIGNet as Shalit et al. (2017) do. The relevant details are stated in Table 5.

Table 4: Hyperparameters of different models in simulation studies.

	Φ_E	Φ_G	Φ_I	π	h^1	h^0	α_1	α_2	batchsize	iteration	learning rate	learning rate for π
Gnet	(100, 100, 100, 100)	–	–	–	(100, 100)	(100, 100)	0.1	–	100	300	$1e^{-3}$	–
Inet	(100, 100, 100, 100)	–	–	(100, 100, 100)	(100, 100)	(100, 100)	–	0.1	100	300	$1e^{-3}$	$1e^{-4}$
DGNet	(100, 100, 100, 100)	(100, 100)	–	–	(100, 100)	(100, 100)	0.1	–	100	300	$1e^{-3}$	–
DINet	(100, 100, 100, 100)	–	(100, 100)	(100, 100, 100)	(100, 100)	(100, 100)	–	0.1	100	300	$1e^{-3}$	$1e^{-4}$
DIGNet	(100, 100, 100, 100)	(100, 100)	(100, 100)	(100, 100, 100)	(100, 100)	(100, 100)	0.1	0.1	100	300	$1e^{-3}$	$1e^{-4}$

Table 5: Hyperparameters of different models in IHDP experiments.

	Φ_E	Φ_G	Φ_I	π	h^1	h^0	α_1	α_2	batchsize	iteration	learning rate	learning rate for π
Gnet	(100, 100, 100, 100)	–	–	–	(100, 100, 100)	(100, 100, 100)	1	–	100	600	$1e^{-3}$	–
Inet	(100, 100, 100, 100)	–	–	(200, 200, 200)	(100, 100, 100)	(100, 100, 100)	–	1	100	600	$1e^{-3}$	$1e^{-3}$
DGNet	(100, 100, 100, 100)	(100, 100)	–	–	(100, 100, 100)	(100, 100, 100)	1	–	100	600	$1e^{-3}$	–
DINet	(100, 100, 100, 100)	–	(100, 100)	(200, 200, 200)	(100, 100, 100)	(100, 100, 100)	–	1	100	600	$1e^{-3}$	$1e^{-3}$
DIGNet	(100, 100, 100, 100, 100, 100)	(100, 100, 100)	(100, 100, 100)	(200, 200, 200)	(100, 100, 100)	(100, 100, 100)	0.1	1	100	600	$1e^{-3}$	$1e^{-3}$

Device. All the experiments are run on Dell 7920 with 1x 16-core Intel Xeon Gold 6250 3.90GHz CPU and 3x NVIDIA Quadro RTX 6000 GPU.

Table 6: Additional comparisons on IHDP dataset.

	Training set		Test set	
	$\sqrt{\epsilon_{PEHE}}$	ϵ_{ATE}	$\sqrt{\epsilon_{PEHE}}$	ϵ_{ATE}
OLS/LR$_1$ (Johansson et al., 2016)	$5.8 \pm .3$	$.73 \pm .04$	$5.8 \pm .3$	$.94 \pm .06$
OLS/LR$_2$ (Johansson et al., 2016)	$2.4 \pm .1$	$.14 \pm .01$	$2.5 \pm .1$	$.31 \pm .02$
k-NN (Crump et al., 2008)	$2.1 \pm .1$	$.14 \pm .01$	$4.1 \pm .2$	$.79 \pm .05$
BART (Chipman et al., 2010)	$2.1 \pm .1$	$.23 \pm .01$	$2.3 \pm .1$	$.34 \pm .02$
CF (Wager & Athey, 2018)	$3.8 \pm .2$	$.18 \pm .01$	$3.8 \pm .2$	$.40 \pm .03$
CEVAE (Louizos et al., 2017)	$2.7 \pm .1$	$.34 \pm .01$	$2.6 \pm .1$	$.46 \pm .02$
SITE (Yao et al., 2018)	$.69 \pm .0$	$.22 \pm .01$	$.75 \pm .0$	$.24 \pm .01$
GANITE (Yoon et al., 2018)	$1.9 \pm .4$	$.43 \pm .05$	$2.4 \pm .4$	$.49 \pm .05$
BLR (Johansson et al., 2016)	$5.8 \pm .3$	$.72 \pm .04$	$5.8 \pm .3$	$.93 \pm .05$
BNN (Johansson et al., 2016)	$2.2 \pm .1$	$.37 \pm .03$	$2.1 \pm .1$	$.42 \pm .03$
TARNet (Shalit et al., 2017)	$.88 \pm .0$	$.26 \pm .01$	$.95 \pm .0$	$.28 \pm .01$
CFR-Wass (GNet) (Shalit et al., 2017)	$.73 \pm .0$	$.12 \pm .01$	$.81 \pm .0$	$.15 \pm .01$
Dragonnet (Shi et al., 2019)	$1.3 \pm .4$	$.14 \pm .01$	$1.3 \pm .5$	$.20 \pm .05$
DKLITE (Zhang et al., 2020)	$.52 \pm .0$	–	$.65 \pm .03$	–
CFR-ISW (Hassanpour & Greiner, 2019a)	–	–	$.70 \pm .0$	$.19 \pm .03$
BWCFR-OW (Assaad et al., 2021)	–	–	$.65 \pm .0$	$.18 \pm .01$
BWCFR-MW (Assaad et al., 2021)	–	–	$.63 \pm .0$	$.19 \pm .01$
BWCFR-TruncIPW (Assaad et al., 2021)	–	–	$.63 \pm .0$	$.19 \pm .01$
MBRL (Huang et al., 2022a)	$.52 \pm .0$	$.12 \pm .01$	$.57 \pm .0$	$.13 \pm .01$
DIGNet (Ours)	$\mathbf{.42 \pm .0}$	$\mathbf{.11 \pm .01}$	$\mathbf{.45 \pm .0}$	$\mathbf{.12 \pm .01}$

Additional results The selection bias of different simulated datasets is illustrated in Figure 5. We compare DIGNet with more baselines in Table 6. Note that $-$ indicates either the code is not released or the original paper does not report relevant values.

A.5 Objectives for Different Models

Objective of GNet.

$$\min_{\Phi_E, h^t} \quad \mathcal{L}_y(\mathbf{x}, \mathbf{t}, \mathbf{y}; \Phi_E, h^t) + \alpha_1 \mathcal{L}_G(\mathbf{x}, \mathbf{t}; \Phi_E).$$

Objective of INet.

$$\begin{aligned} \max_{\pi} \quad & \alpha_2 \mathcal{L}_I(\mathbf{x}, \mathbf{t}; \Phi_E, \pi), \\ \min_{\Phi_E, h^t} \quad & \mathcal{L}_y(\mathbf{x}, \mathbf{t}, \mathbf{y}; \Phi_E, h^t) + \alpha_2 \mathcal{L}_I(\mathbf{x}, \mathbf{t}; \Phi_E, \pi). \end{aligned}$$

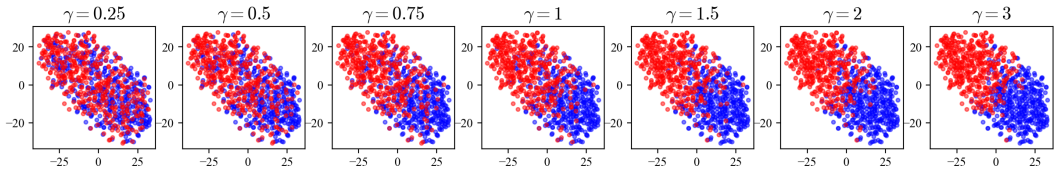

Figure 5: T-SNE visualizations of the covariates as γ varies. Red represents the treatment group and blue represents the control group. A larger γ indicates a greater imbalance between the two groups.

Objective of DINet. Note that similar to DIGNet, the pre-balancing patterns are preserved by only updating Φ_I but fixing Φ_E in the second step.

$$\begin{aligned} \max_{\pi} \quad & \alpha_2 \mathcal{L}_I(\mathbf{x}, \mathbf{t}; \Phi_I \circ \Phi_E, \pi), \\ \min_{\Phi_I} \quad & \alpha_2 \mathcal{L}_I(\mathbf{x}, \mathbf{t}; \Phi_I \circ \Phi_E, \pi), \\ \min_{\Phi_E, \Phi_I, h^t} \quad & \mathcal{L}_y(\mathbf{x}, \mathbf{t}, \mathbf{y}; \Phi_E \oplus (\Phi_I \circ \Phi_E), h^t). \end{aligned}$$

Objective of DGNet. Note that similar to DIGNet, the pre-balancing patterns are preserved by only updating Φ_G but fixing Φ_E in the first step.

$$\begin{aligned} \min_{\Phi_G} \quad & \alpha_1 \mathcal{L}_G(\mathbf{x}, \mathbf{t}; \Phi_G \circ \Phi_E), \\ \min_{\Phi_E, \Phi_G, h^t} \quad & \mathcal{L}_y(\mathbf{x}, \mathbf{t}, \mathbf{y}; \Phi_E \oplus (\Phi_G \circ \Phi_E), h^t). \end{aligned}$$

Objective of DIGNet.

$$\begin{aligned} \min_{\Phi_G} \quad & \alpha_1 \mathcal{L}_G(\mathbf{x}, \mathbf{t}; \Phi_G \circ \Phi_E), \\ \max_{\pi} \quad & \alpha_2 \mathcal{L}_I(\mathbf{x}, \mathbf{t}; \Phi_I \circ \Phi_E, \pi), \\ \min_{\Phi_I} \quad & \alpha_2 \mathcal{L}_I(\mathbf{x}, \mathbf{t}; \Phi_I \circ \Phi_E, \pi), \\ \min_{\Phi_E, \Phi_I, \Phi_G, h^t} \quad & \mathcal{L}_y(\mathbf{x}, \mathbf{t}, \mathbf{y}; \Phi_E \oplus (\Phi_I \circ \Phi_E) \oplus (\Phi_G \circ \Phi_E), h^t). \end{aligned}$$